Journal of Colloid and Interface Science 538 (2019) 660–670

Contents lists available at ScienceDirect

Journal of Colloid and Interface Science

journal homepage: www.elsevier.com/locate/jcis

Regular Article

Properties of the micelles of sulfonated methyl esters determined from the stepwise thinning of foam films and by rheological measurements

Elka S. Basheva [a], Krassimir D. Danov [a], Gergana M. Radulova [a], Peter A. Kralchevsky [a,*], Hui Xu [b], Yee Wei Ung [b], Jordan T. Petkov [b,1]

[a] Department of Chemical and Pharmaceutical Engineering, Faculty of Chemistry and Pharmacy, Sofia University, 1164 Sofia, Bulgaria
[b] KLK Oleo, KL-Kepong Oleomas SDN BHD, Menara KLK, Jalan PJU 7/6, Mutiara Damansara, 47810 Petaling Jaya, Selangor Dalur Ehsan, Malaysia

GRAPHICAL ABSTRACT

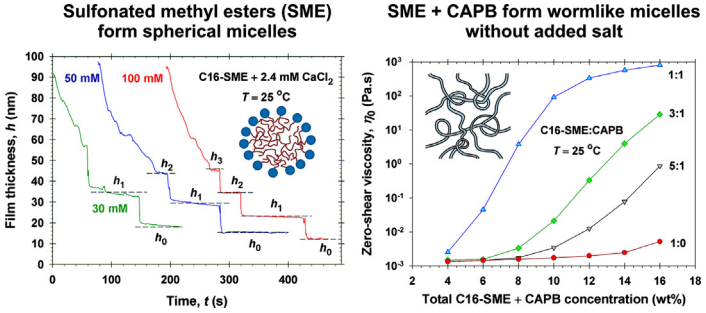

ARTICLE INFO

Article history:
Received 14 October 2018
Revised 9 December 2018
Accepted 10 December 2018
Available online 11 December 2018

Keywords:
Sulfonated methyl esters
Micelle aggregation number
Stratifying foam films
Film thicknesses interpretation
Rheology of micellar solutions
Wormlike micelles

ABSTRACT

Hypotheses: The micellar solutions of sulfonated methyl esters (SME) are expected to form stratifying foam films that exhibit stepwise thinning. From the height of the steps, which are engendered by micellar layers confined in the films, we could determine the micelle aggregation number, surface electric potential, and ionization degree. Moreover, addition of the zwitterionic surfactant cocamidopropyl betaine (CAPB) is expected to transform the small spherical micelles of SME into giant wormlike aggregates.
Experiments: Stratifying films from SME solutions are formed and the heights of the steps are recorded. The viscosity of mixed SME + CAPB solutions is measured at various concentrations and weight ratios of the two surfactants.
Findings: By theoretical analysis of the foam film data, we established that at 30–100 mM SME spherical micelles are formed and their aggregation number was determined. The addition of calcium ions, as in hard water, does not produce significant effect. However, SME and CAPB exhibit a strong synergism with respect to micelle growth as indicated by the high solution's viscosity. For this reason, the SME + CAPB mixtures represent a promising system for formulations in personal-care and house-hold detergency, having in mind also other useful properties of SME, such as high hard water tolerance, biodegradability and skin compatibility.

1. Introduction

Here, on the basis of data for the stepwise thinning of foam films, we determine the aggregation number, N_{agg}, surface electrostatic potential, φ, and ionization degree, α, of the spherical

* Corresponding author.
E-mail address: pk@lcpe.uni-sofia.bg (P.A. Kralchevsky).
[1] Present address: Arch UK Biocides Ltd., Hexagon Tower, Crumpsall Vale, Blackley, Manchester M9 8GQ, UK.

https://doi.org/10.1016/j.jcis.2018.12.034
0021-9797/

micelles formed in solutions of sulfonated methyl esters (SME). More precisely, we are dealing with α-sulfo fatty acid methyl ester sulfonates, sodium salts, which are also known as methyl ester sulfonates (MES). We report also rheological data, which imply that the mixed solutions of SME and CAPB (cocamidopropyl betaine) undergo a transition from small spherical to giant wormlike micelles.

The sulfonated methyl esters (Fig. 1) are produced from renewable palm-oil based materials or as a by-product from bio-diesel synthesis [1–4]. They have been promoted as alternatives to the petroleum-based surfactants [5]. SMEs exhibit a series of useful properties such as excellent biodegradability and biocompatibility; excellent stability in hard water; good wetting and cleaning performance, and skin compatibility [2,6–11]. The SME surfactants are produced typically with even alkyl chainlengths, from C_{12} to C_{18}. Here, they will be denoted C*n*-SME, $n = 12, 14, 16, 18$.

In the early studies on the interfacial properties of SMEs, the critical micelle concentrations (CMC) of their solutions were determined from data for the surface tension and electric conductivity [12–19]. The CMC values obtained in these studies differ considerably because of the presence of small amounts of nonionic admixtures in the used SME samples. Recent neutron reflectivity measurements [20] and surface tension data processing [21] showed that the correct value of the saturation adsorption of the C*n*-SME molecules at the air-water interface is 3.4 ± 0.1 μmol/m^2, the excluded area per molecule being 37 Å^2. The effect of added NaCl on the CMC of SME solutions was quantified [21]. The binding energy of Ca^{2+} ions to the headgroups of SME turned out to be considerably smaller than to the headgroups of linear alkylbenzene sulfonates (LAS) [22]. As a result, the SMEs possess a much higher hard water tolerance than LAS. The effect of multivalent counterions (Ca^{2+} and Al^{3+}) on the surfactant adsorption was also studied by neutron reflectivity [23,24]. The results for mixtures of SME with different chainlengths showed that the variations in the surface composition are described well by a pseudo phase approximation with repulsive interactions between C16-SME and C18-SME molecules [24].

The rheological studies with micellar solutions of SME [18] showed that the dependence of the zero-shear viscosity, η_0, on the NaCl concentration has a sharp maximum, which indicates the growth of wormlike micelles to the left of the peak, and transition to self-assemblies with another structure to the right of the peak.

In our previous study [21], we determined the dependence of CMC of C*n*-SME on the number of carbon atoms in the alkyl chain, *n*, and on the NaCl concentration. Here, our goal is to extend this analysis to characterization of the C*n*-SME micelles with respect to their aggregation number, surface electric charge and potential. For this goal, the method developed in Ref. [25], which is based on theoretical analysis of data for stratifying foam films containing layers of surfactant micelles, is applied; see also Refs. [26–28].

The stepwise thinning (stratification) of foam films is a manifestation of the action of the oscillatory structural force, which becomes significant if the effective volume fraction of surfactant micelles (or other colloidal particles) exceeds ca. 15 vol% [28,29]. It should be noted that premicellar aggregates could be present in the liquid films at concentrations below the CMC [30], but they do not form ordered layers and do not give rise to oscillatory forces. The first explanation of the stepwise transitions as a layer-by-layer thinning of an ordered structure of spherical micelles was given by Nikolov et al. [31–33]. Cryo-electron microscopy pictures of vitrified stratifying films at various stages of their evolution [34,35] directly proved that the stepwise transitions are due to the presence of ordered micellar layers inside the film and represent layer-by-layer drainage of the film.

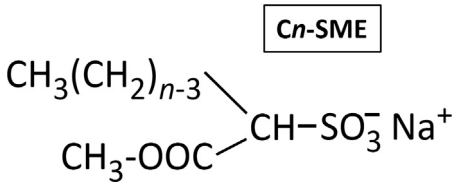

Fig. 1. Structural formula of C*n*-SME.

It should be noted that stratifying films from SME solutions have not been investigated so far. To the best of our knowledge, systematic study on the properties of SME micelles, such as aggregation number, ionization degree and surface electric potential and their dependences on the surfactant chainlength and concentration is still missing. There is a single estimate based on static light scattering data that $N_{agg} \approx 50$ [36], but the dependence of N_{agg} on chainlength and concentration has not been studied.

The paper is organized as follows. Section 2 presents the used materials and methods. Section 3 presents the experimental results for stratifying liquid films. In Section 4.1, the obtained data are analyzed theoretically and the values of micelle aggregation number, ionization degree and surface electric potential, as well as their dependences on the surfactant chainlength and concentration, are determined. In Section 4.2, we present an independent verification of the used theoretical model against experimental data for the equilibrium film thickness. In Section 4.3, the packing parameter is estimated for different SME chainlengths in relation to the possibility for formation of micelles of different shapes. Finally, in Section 5 we examine the effect of added zwitterionic surfactant, CAPB, to check whether growth of giant wormlike micelles occurs with SME, as this happens with other anionic surfactants.

2. Materials and methods

2.1. Materials

Sulfonated methyl esters (SME) with three different alkyl chains, C12, C14, and C16, produced by the Malaysian Palm Oil Board (MPOB) and KLK OLEO, were used in our experiments. The mollar masses and the purities of the used samples are $M = 316$ g/mol and 97.4% for C12-SME; $M = 344$ g/mol and 97.9% for C14-SME; $M = 372$ g/mol and 96.0% for C16-SME [21,22]. The amount of water in the used samples was established by Karl Fisher analysis and taken into account when calculating the surfactant concentrations. In addition, by electric conductivity measurements we estimated the concentrations of NaCl admixture in the used samples relative to the surfactant: 16 mol% in C12-SME; 14 mol% in C14-SME, and 24 mol% in C16-SME. These samples were used in our experiments without further purification. The measured foam-film thicknesses and viscosities of micellar solutions are affected by the NaCl-admixture in C*n*-SME. The effect of admixtures is taken into account in all theoretical calculations presented in this paper.

The experimental surface tension isotherms have well pronounced minima, which indicate the presence of small amounts of nonionic surface active admixtures, presumably unsulfonated methyl esters and fatty acids [21]. At concentrations above the CMC, these admixtures are solubilized in the micelles of SME and (as demonstrated below) their effect on the foam film thickness and micelle properties is negligible.

The zwitterionic surfactant cocamidopropyl betaine (CAPB), $M = 356$ g/mol, product of Evonik, commercial name Tego® Betain F50, was also used. The CMC of CAPB at 25 °C is 0.09 mM. By conductivity measurements, we established that 100 mM CAPB contains 120 mM NaCl in the used sample. Such high content of

NaCl is typical for the commercially available CAPB samples [45,46]. The presence of NaCl admixtures in both C*n*-SME and CAPB has been taken into account when interpreting theoretically the experimental data.

In some experiments, we used also calcium chloride, $CaCl_2 \cdot 6H_2O$ (≥99%), and sodium hydroxide, NaOH (>99%), both of them products of Sigma-Aldrich, as well as myristic (tetradecanoic) acid HC14 (≥98% from Fluka) and palmitic (hexadecanoic) acid HC16 (>98% from Riedel-de-Haën). The solutions were prepared with deionized water of specific resistivity 18.2 MΩ·cm purified by Elix 3 water purification system (Millipore). All experiments were carried out at a temperature of 25 °C.

2.2. Methods

Scheludko-Exerowa (SE) capillary cell [37,38] was used to study the drainage and evolution of foam films. Experiments with SE cell have been used to model the bubble-bubble interactions in foams [38] and the bubble-interface interactions [39], as well as to investigate dynamic phenomena in thin liquid films [40], including the phenomenon stratification [25,26,31,32]. The inner radius of the capillary cell was R_{in} = 1.5 mm and the applied capillary pressure was between 60 and 80 Pa. The SE cell is closed in a container, so that the water vapors are equilibrated with the studied solution and evaporation from the film is prevented. After a foam film is formed, its thickness decreases with time because of the drainage of liquid out of the film. The film thickness was determined interferometrically, from the measured intensity of light reflected from the film surfaces, which was registered by a photomultiplier and recorded by a computer in the course of the experiment. Monochromatic light of wavelength λ = 546 nm was used.

The so-called equivalent water thickness of the film, h_w, is determined assuming that the whole film consists of water of refractive index n_f = 1.333 [41,42]:

$$h_w = \frac{\lambda}{2\pi n_f}[k\pi + \arcsin(\Delta^{1/2})] \tag{1}$$

$$\Delta \equiv b\left[1 + \frac{4a(1-b)}{(1-a)^2}\right]^{-1}, \quad a \equiv \left(\frac{n_f - n_0}{n_f + n_0}\right)^2, \quad b \equiv \frac{I - I_{min}}{I_{max} - I_{min}} \tag{2}$$

where I_{max} and I_{min} denote the maximum and minimum intensity of the reflected light; k = 0, 1, 2, … is the order of the interference maxima; λ is the wavelength of the used monochromatic light; n_0 is the refractive index of the outer phase (in our case – air, n_0 = 1). Note that for n_f = 1.333 and n_0 = 1, the approximation $\Delta \approx b$ leads to a relative error that does not exceed 4%.

The equivalent water thickness of the film, h_w, is slightly greater than the real film thickness, h. In the case of dense surfactant adsorption layers, h can be estimated as follows (see Fig. 2):

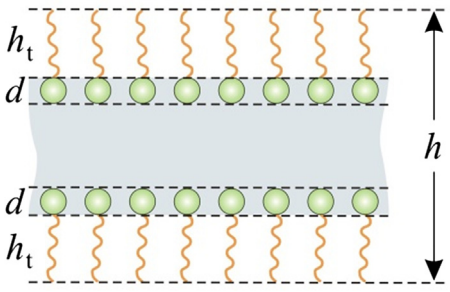

Fig. 2. The model of foam film used to determine the actual film thickness h; the length of the surfactant tail is denoted h_t and d is the diameter of the surfactant headgroup.

$$h = h_w - 2h_t\frac{n_t^2 - n_f^2}{n_f^2 - n_0^2} - 2d\frac{n_d^2 - n_f^2}{n_f^2 - n_0^2} \tag{3}$$

where h_w is given by Eqs. (1) and (2); h_t and n_t are the thickness and refractive index of the dense layer of surfactant tails, whereas d and n_d are the thickness and the mean refractive index of the layer of surfactant headgroups. In the case of complete surface coverage, one could use the value n_t = 1.42. For sulfate or sulfonate headgroups immersed in water, one could use the value n_d = 1.394 for sodium sulfate decahydrate. The Tanford expression [43]

$$h_t \equiv l = (0.154 + 0.1265n)\ \text{nm} \tag{4}$$

relates the extended length of the hydrocarbon tail, l, with the number of the carbon atoms in the tail, n. The diameter of the surfactant headgroup is d = 0.68 nm [21]. Thus, from Eqs. (3) and (4) one obtains $h = (h_w - 1.32)$ nm for C12-SME; $h = (h_w - 1.48)$ nm for C14-SME, and $h = (h_w - 1.68)$ nm for C16-SME. The correction terms affect the values of the film thickness, h, but they do not affect the heights of the stratification steps, Δh (see below).

Rheological measurements were carried out with mixed solutions of C*n*-SME and CAPB. For this purpose, a rotational rheometer Bohlin Gemini (Malvern Instruments, UK) was used in steady-shear regime. The experiments were carried out with a cone-and-plate geometry. For viscosity lower than 40 Pa·s, the cone angle was 2° and the minimal gap distance was 70 μm; for higher viscosity, the angle and distance were, respectively, 4° and 150 μm. The temperature of 25 °C was controlled by a Peltier element and the evaporation was suppressed by a solvent trap. The shear stress, τ, was measured as a function of the applied shear rate, $\dot{\gamma}$. Furthermore, the apparent viscosity, $\eta(\dot{\gamma})$, was calculated from the equation $\eta = \tau/\dot{\gamma}$. The experimental shear rate varied from 0.01 to 100 s^{-1}. The zero-shear viscosity, η_0, represents the limiting value of η at $\dot{\gamma} \to 0$. This is a typical experimental protocol used to study the rheology of concentrated micellar solutions [44–47].

3. Experimental results

As an example of the observed processes, Fig. 3 shows photographs of consecutive stages of thinning of a foam film formed from 100 mM C16-SME solution in the SE cell. The stepwise decreasing of film thickness (stratification) takes place through the formation and expansion of spots of different thickness h_j, which corresponds to a film containing j micellar layers (j = 0, 1, 2, 3, …) [32,48]. With the decrease of film thickness, the spots look darker in reflected light. Thus, Fig. 3a shows the appearance of a spot of thickness h_3 that contains three micellar layers. This spot expands and covers the whole film area. Next, a spot of thicknesses h_2, which contains two micellar layers, appears and expands (Fig. 3b). Furthermore, a film with one micellar layer and thickness h_1 is formed (Fig. 3c), and finally a stable black film of thickness h_0 appears (Fig. 3d) and covers the whole film area. The Newton interference rings around the film are the most pronounced in Fig. 3d, which indicates a rise of the film contact angle with the decrease of film thickness [48].

The light reflected from the film is transmitted to a photomultiplier by an optical fiber. When the front of a darker expanding spot (Fig. 3) passes before the optical fiber, the photomultiplier registers a drop of intensity of the reflected light, I, which is converted into film thickness, h, by using Eqs. (1)–(3). As an example, Fig. 4 shows experimental dependencies of h on time, t, obtained with foam films from C16-SME solutions in the SE cell. Similar experimental results for C12- and C14-SME are shown in Appendix A; see Figs. A1 and A2 therein.

Fig. 4a shows h-vs.-t curves obtained at three different concentrations of C16-SME, viz. C_S = 30, 50 and 100 mM. One sees that the number of stepwise transitions increases and the height of the

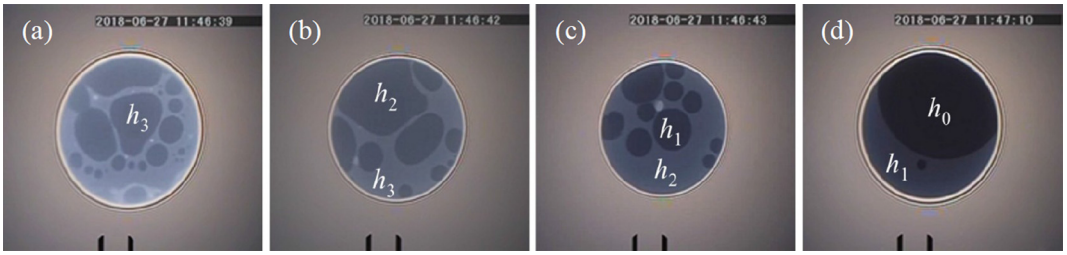

Fig. 3. Consecutive stages of stepwise thinning of a liquid film formed form 100 mM C16-SME solution: (a) appearance of film with three micelle layers and thickness h_3; (b) transition to film with two micelle layers and thickness h_2; (c) transition to film with one micelle layer and thickness h_1, and (d) transition to an electrostatically stabilized film of thickness h_0, which does not contain micellar layers. The scaling mark is 50 μm.

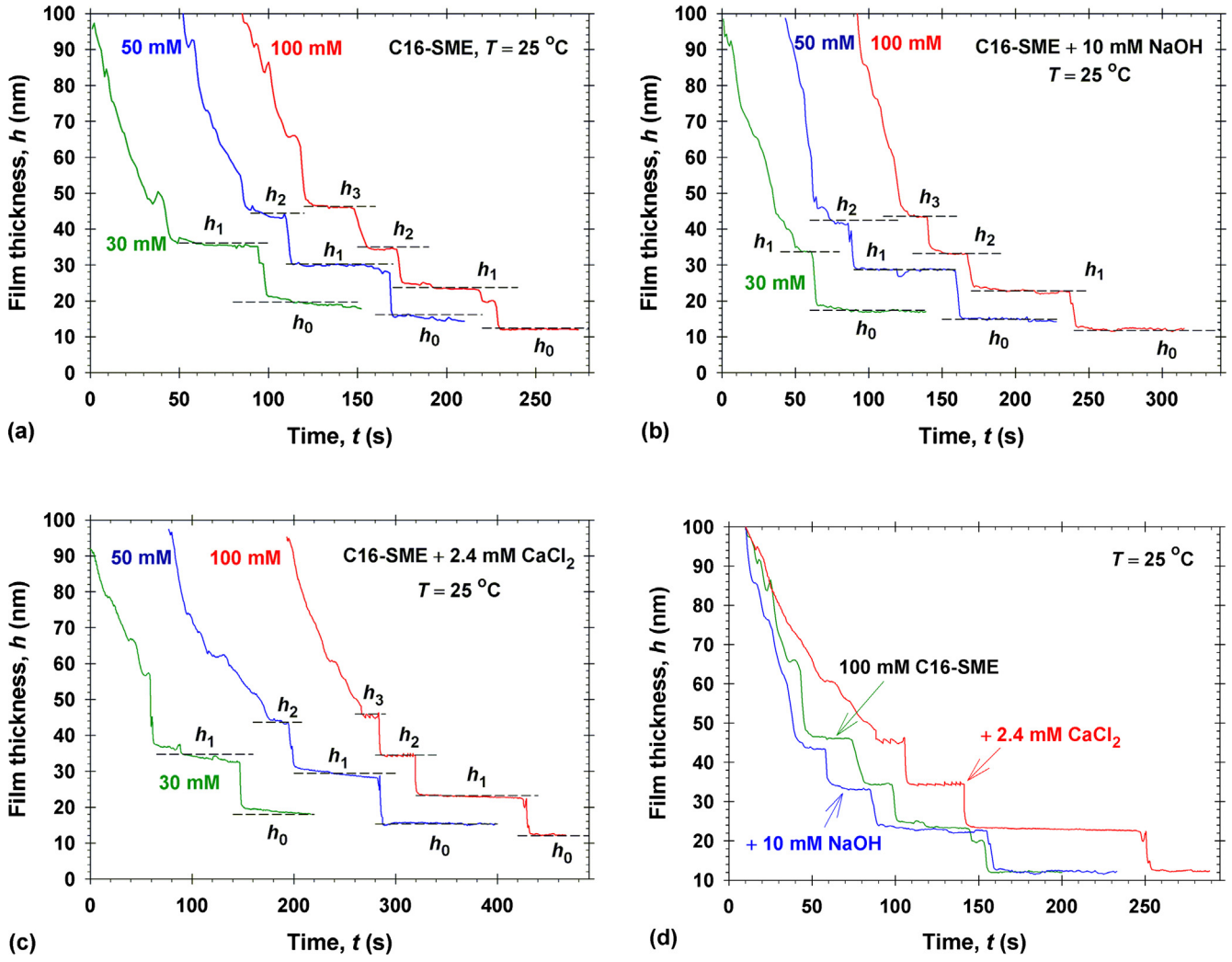

Fig. 4. Experimental dependencies of the film thickness, h, on time, t, for foam films formed in a SE cell from C16-SME solutions of concentrations denoted in the figure: (a) C16-SME alone; (b) with added 10 mM NaOH; (c) with added 2.4 mM $CaCl_2$; (d) comparison of the three drainage curves at 100 mM C16-SME.

step, $\Delta h = h_j - h_{j-1}$, decreases with the rise of surfactant concentration. As known from previous experiments with ionic surfactant micelles [25,28], at a given surfactant concentration, C_S, Δh is independent of the order of the step, j. Fig. 4b shows similar h-vs.-t curves obtained in the presence of 10 mM NaOH, which was added to suppress the effect of fatty acid admixtures in the used SME sample. Fig. 4c presents similar curves, but obtained in the presence of 2.4 mM $CaCl_2$, which was added to investigate the effect of water hardness on the film stratification.

The comparison of the drainage curves for films formed from 100 mM Cn-SME (see Fig. 4d, A1d and A2d) shows that the drainage is the fastest for the films with NaOH, whereas the drainage is the slowest for the films with $CaCl_2$. In the latter case, the Ca^{2+} counterions neutralize more efficiently the electrostatic repulsion between the headgroups of the adsorbed SME molecules, which leads to more densely packed adsorption layers [22] that become more rigid (almost tangentially immobile) and slow down the film drainage [49]. In contrast, the added NaOH ionizes the admixtures

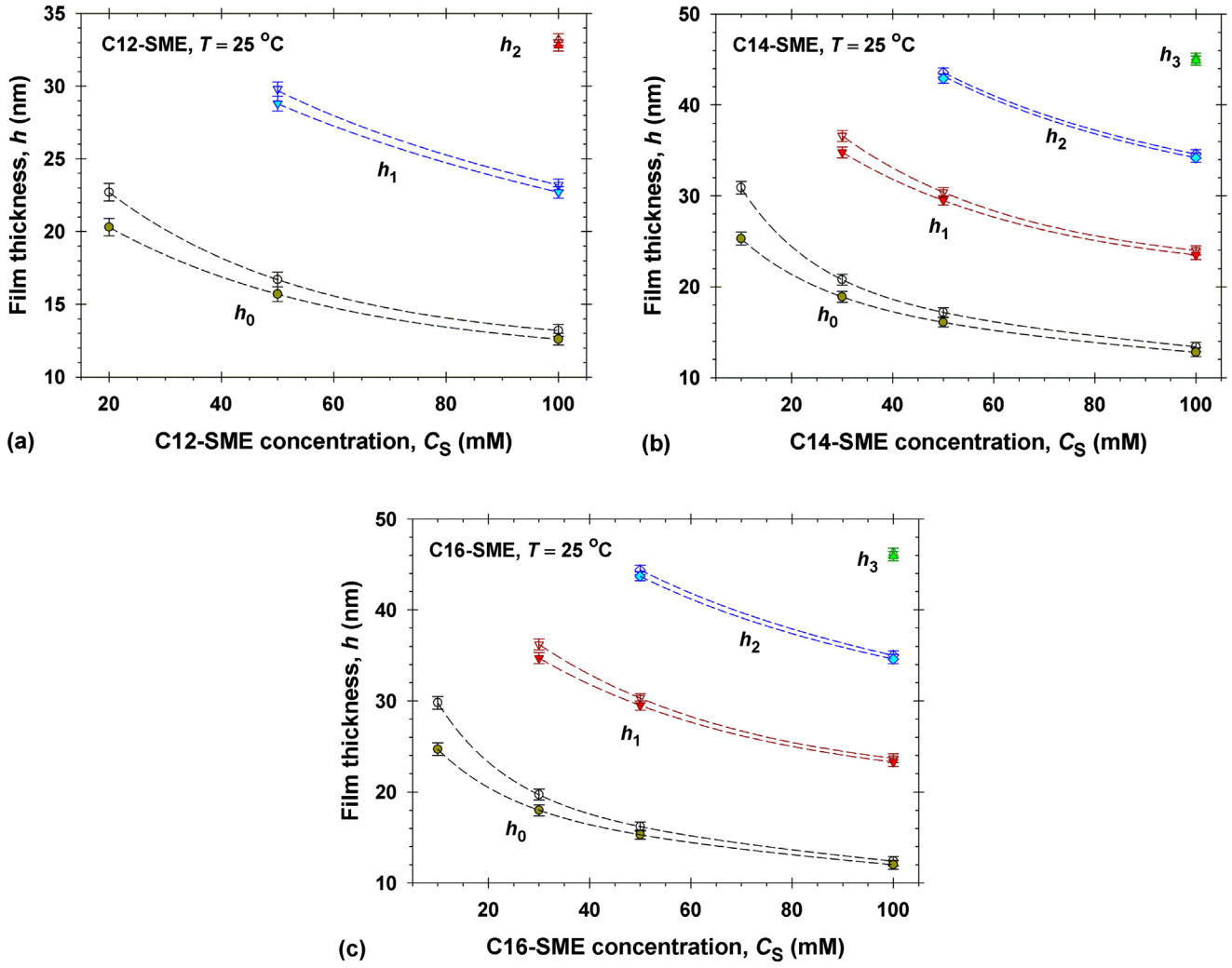

Fig. 5. Dependence of the experimental film thickness h_j, corresponding to j = 0, 1, 2, and 3 layers of micelles in the film, on the SME concentration: (a) C12-SME; (b) C14-SME, and (c) C16-SME. For each h_j, the upper curves with empty symbols and the lower curves with full symbols correspond to solutions with 0 and 2.4 mM $CaCl_2$, respectively. The lines are guides to the eye.

of fatty acids, which leads to lower surface dilatational elasticity and faster film drainage. The effect of NaOH is smaller than that of Ca^{2+}, because the amount of fatty acid admixtures in SME is relatively low [21].

Fig. 5 summarizes the results from all experiments with stratifying films from C*n*-SME solutions without and with added $CaCl_2$. As seen in the figure, the effect of 2.4 mM $CaCl_2$ on the values of the film thickness is not so significant. (The effect of $CaCl_2$ on the film drainage time in Fig. 4d is more significant). The values of h_j for the solutions with added 10 mM NaOH turned out to be practically the same as those with 2.4 mM $CaCl_2$; see Fig A3 in Appendix A.

The data for h_j (j = 0,1,2,3) shown in Fig. 5 serve as a basis for determining the micellar properties (see below). For this reason, the values of h_j were experimentally determined with a high precision. Each value of h_j in Figs. 5 and A3 represents the average from at least 30 measurements of h-vs.-t curves, like those in Fig. 4. As seen in Fig. 5, the error bars are relatively small.

As already mentioned, for a solution of given composition the heights of the steps are equal in the framework of the experimental error: $h_3 - h_2 \approx h_2 - h_1 \approx h_1 - h_0 \approx \Delta h$. From the values of Δh, the micelle aggregation number, N_{agg}, surface electrostatic potential, φ, and ionization degree, α, have been determined. The obtained mean values of Δh and h_0 for C*n*-SME without and with additives are listed in the second and third columns of Table 1. The values of h_0 serve for an independent verification of the model used to calculate N_{agg}, φ, and α. The values of Δh in Table 1 are more than two times greater than the micelle hydrodynamic diameter that can be estimated as $2(h_t + d)$; see Fig. 2 and the related text. This difference is due to the fact that the electric double-layer around the micelle contributes to Δh [28,32].

To verify whether small amounts of nonionic surfactant admixtures can influence the thickness of the investigated films, we measured the final equilibrium film thickness, h_0, vs. the C16-SME concentration, C_S, for several different concentrations of added fatty acids: 0, 4 and 8 mol% palmitic acid (HC16), and 8 mol% myristic acid (HC14) relative to the C16-SME.

The pH of the studied solutions is ≈5, so that a considerable part of the added fatty acid is present in protonated (nonionic) form. The experimental results, which are shown in Fig. 6, refer to concentrations above the CMC and indicate that the presence of small nonionic admixtures produces a negligible effect on the equilibrium film thickness, h_0.

It should be noted that the presence of NaCl as an admixture in C*n*-SME contributes to the screening of electrostatic repulsion, which has affected the experimental values of Δh and h_0 in Table 1;

Table 1
Measured step height, Δh, and final film thickness, h_0, and calculated concentration of surfactant monomers, c_1, micelle surface electrostatic potential, φ, degree of ionization, α, and aggregation number, N_{agg}, for micellar solutions of C*n*-SME.

C_S (mM)	Δh (nm)	h_0 (nm)	c_1 (mM)	$-\varphi$ (mV)	α	N_{agg}	N_{max}
C12-SME							
50	13.1 ± 0.15	16.7 ± 0.20	8.50	99.6	0.240	56 ± 1.9	56
100	10.0 ± 0.11	13.2 ± 0.15	5.94	93.5	0.208	57 ± 1.9	56
C12-SME + 2.4 mM $CaCl_2$							
50	13.1 ± 0.16	15.7 ± 0.19	7.33	96.8	0.228	58 ± 2.1	56
100	10.1 ± 0.12	12.6 ± 0.14	5.37	91.5	0.201	59 ± 2.1	56
C12-SME + 10 mM NaOH							
50	13.0 ± 0.15	15.3 ± 0.15	6.92	95.7	0.224	57 ± 2.0	56
100	10.0 ± 0.12	12.4 ± 0.14	5.16	90.7	0.198	57 ± 2.1	56
C14-SME							
30	15.8 ± 0.19	20.8 ± 0.22	1.45	109	0.287	68 ± 2.5	74
50	13.2 ± 0.16	17.2 ± 0.20	1.06	103	0.255	68 ± 2.5	74
100	10.6 ± 0.12	13.4 ± 0.16	0.677	97.3	0.216	71 ± 2.4	74
C14-SME + 2.4 mM $CaCl_2$							
30	15.9 ± 0.19	18.9 ± 0.20	1.10	104	0.262	70 ± 2.5	74
50	13.4 ± 0.16	16.1 ± 0.20	0.869	99.4	0.239	71 ± 2.5	74
100	10.7 ± 0.13	12.8 ± 0.15	0.602	93.1	0.207	73 ± 2.7	74
C14-SME + 10 mM NaOH							
30	15.6 ± 0.18	18.2 ± 0.19	0.996	102	0.254	66 ± 2.3	74
50	13.1 ± 0.15	15.7 ± 0.18	0.808	98.0	0.234	67 ± 2.3	74
100	10.5 ± 0.12	12.6 ± 0.14	0.575	92.1	0.204	69 ± 2.4	74
C16-SME							
30	16.5 ± 0.20	19.7 ± 0.20	0.141	107	0.280	81 ± 2.9	94
50	14.1 ± 0.18	16.2 ± 0.19	0.0996	101	0.246	84 ± 3.2	94
100	11.3 ± 0.15	12.4 ± 0.13	0.0620	92.0	0.206	87 ± 3.5	94
C16-SME + 2.4 mM $CaCl_2$							
30	16.7 ± 0.20	18.0 ± 0.20	0.109	102	0.257	84 ± 3.0	94
50	14.2 ± 0.18	15.3 ± 0.18	0.0836	97.1	0.232	86 ± 3.3	94
100	11.3 ± 0.14	12.0 ± 0.14	0.0561	90.0	0.199	87 ± 3.2	94
C16-SME + 10 mM NaOH							
30	16.3 ± 0.20	17.4 ± 0.18	0.0994	100	0.249	78 ± 2.9	94
50	13.8 ± 0.17	14.9 ± 0.16	0.0783	95.8	0.227	79 ± 2.9	94
100	11.0 ± 0.13	11.8 ± 0.12	0.0539	89.2	0.196	80 ± 2.8	94

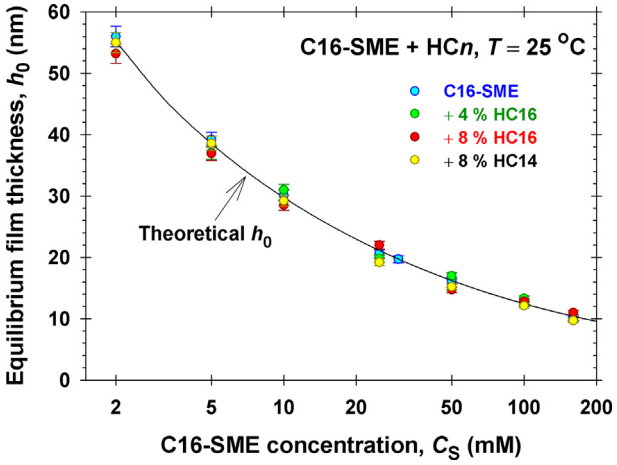

Fig. 6. Plot of experimental data for the final equilibrium film thickness, h_0, vs. the C16-SME concentration, C_S, at several different concentrations of added fatty acids denoted in the figure. The theoretical solid line is drawn without using any adjustable parameters; see the text.

they are lower than they would be in the absence of NaCl. (Note, however, that the predominant part of Na^+ counterions in the studied solutions originates from the dissociation of C*n*-SME molecules.) Hence the values of N_{agg} in Table 1, which are calculated from the measured Δh (see below), refer to the experimental C*n*-SME samples, which contain NaCl admixtures. The presence of such admixtures is taken into account in our theoretical calculations of the surfactant monomer concentration, c_1; micelle surface potential, φ, and ionization degree, α; see Table 1 and Section 4. The theoretically predicted dependence of h_0 on the SME concentration, C_S, is in excellent agreement with the experimental h_0 vs. C_S dependence; see Section 4.2.

4. Theoretical section

4.1. Estimation of N_{agg}, φ and α

For electrically charged spherical micelles (and more generally – colloidal particles), the height of the stratification steps, Δh, is simply connected to the micelle bulk number concentration, c_{mic}, viz. $\Delta h = c_{mic}^{-1/3}$. This law has been experimentally established in a series of studies with thin foam films using the SE cell [31,32]; by CP-AFM measurements supported by SANS and SAXS experiments [50–54], as well as theoretically predicted by density functional calculations and MC simulations [50–55]. In the case of extended polyelectrolyte chains of concentration c_p, another law, $\Delta h \propto c_p^{-1/2}$, has been found experimentally [56,57].

The micelle concentration can be expressed as $c_{mic} = (C_S - c_1)/N_{agg}$ where, as usual, C_S is the total input surfactant concentration and c_1 is the concentration of surfactant monomers in equilibrium with the micelles, both of them expressed as number of molecules per unit volume. Then, from the relation $\Delta h = c_{mic}^{-1/3}$ one derives [25,28]:

$$N_{agg} = (C_S - c_1)(\Delta h)^3 \quad (5)$$

Eq. (5) enables one to determine the mean micelle aggregation number, N_{agg}, from the experimental height of the step, Δh. In Refs. [25,28], Eq. (5) with $c_1 \approx$ CMC was used to estimate the aggregation number of several ionic surfactants from the measured Δh. The relation $c_1 \approx$ CMC is a good approximation for surfactants of low CMC, for which stratification is observed at $C_S \gg$ CMC. However, this is not a good approximation for surfactants with relatively high CMC, like C12-SME, for which CMC = 14.1 mM [21]. In addition, the relation c_1 = CMC is satisfied at the critical micellization concentration, where the first micelles appear. However, stratifying films are observed at surfactant concentrations, which are considerably higher than the CMC. At such concentrations, c_1 < CMC, insofar as the concentration of surfactant monomers, c_1, decreases with the rise of C_S at C_S > CMC [58].

To achieve accurate determination of N_{agg} from Eq. (5) and to find out how significant is the decrease of c_1 at concentrations above the CMC, we applied the complete micellization theory from Ref. [58], as described in Appendix B. This task is facilitated by the fact that all necessary micellization parameters have been already determined in Ref. [21]; see Table B1 in Appendix B. The micellization theory from Ref. [58] yields also the other two parameters of interest: the micelle surface electric potential, φ, and the micelle degree of ionization, α. Furthermore, one could find the micelle electric charge, $q = \alpha N_{agg} e$, where e is the electronic charge.

The values of c_1, φ and α for the investigated micellar solutions, determined as explained in Appendix B, are given in Table 1. Because of the lowering of c_1 at surfactant concentrations above the CMC, the values of c_1 in the investigated concentration range are markedly lower than the CMC values, which are 14.1, 4.0 and 1.1 mM, for C12-, C14- and C16-SME, respectively [21]. In view of Eq. (5), this effect is important for C12-SME, for which the calculated variation of c_1 as a function of C_S is shown in Fig. 7. Similar dependencies for C14- and C16-SME are shown in Fig. B1 in Appendix B. As seen in Fig. 7, c_1 decreases from 13.5 mM at C_S = 20 mM to 8 mM at C_S = 100 mM. In other words, even at 100 mM C12-SME, c_1 is 8% of C_S, so that its effect on the calculated N_{agg} is not negligible; see Eq. (5). We calculated also plots of c_1 vs. C_S assuming the presence of nonionic admixtures in C12-SME. As seen in Fig. 7, the effect of these admixtures is rather small, practically negligible.

The physical reason for the decrease of c_1 with the rise of total surfactant concentration (Fig. 7) is the fact that with the increase of C_S the ionic strength of solution, I, also increases owing to the counterions dissociated from the newly formed micelles. The increased ionic strength provides better screening of the electrostatic repulsion between the surfactant molecules incorporated in the micelles, thus, decreasing their electrochemical potential. As a result, the micelle–monomer equilibrium is shifted toward the micelles, i.e. the concentration of surfactant in micellar form increases, whereas the concentration of monomers, c_1, decreases. These processes are described by the system of equations presented in Appendix B.

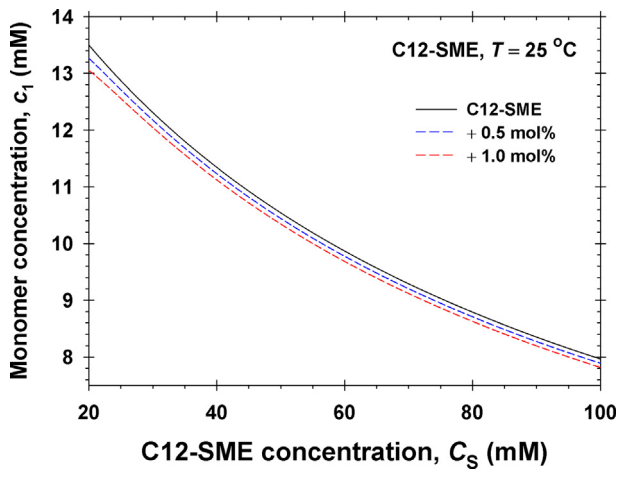

Fig. 7. Calculated surfactant monomer concentration, c_1, as a function of the total C12-SME concentration, C_S, above the CMC for different mol% of nonionic admixture (C12 unsulfonated methyl ester) denoted in the figure.

The solution of the aforementioned system of equations yields also the values of the micelle electrostatic potential φ and ionization degree α; see Table 1. One sees that φ is in the range between 89 and 109 mV and decreases with the rise of total surfactant concentration C_S. φ decreases also with the addition of electrolytes, $CaCl_2$ and NaOH, the effect of NaOH being slightly stronger because of (i) the higher concentration of NaON and (ii) lower binding energy of Ca^{2+} in the Stern layer (to the sulfonate headgroups of SME) as compared to Na^+; see Ref. [22]. In this respect, SME is unique among the anionic surfactants, and this fact correlates with its high hard-water tolerance.

The micelle ionization degree, α, varies in the range between 0.19 and 0.29 (Table 1). This relatively low degree of ionization is due to the binding (adsorption) of Na^+ and Ca^{2+} counterions on the surfactant headgroups expressed on the micelle surface. With the increase of the total surfactant concentration and the concentrations of added electrolytes ($CaCl_2$ and NaOH), α decreases, as it should be expected.

Next, with the values of C_S, Δh and c_1 in Table 1 we calculated the micelle aggregation number, N_{agg}, using Eq. (5). N_{agg} increases with the increase of surfactant chainlength and concentration (Table 1). Thus, N_{agg} varies in the range 56–59 for C12-SME; 67–73 for C14-SME, and 78–87 for C16-SME. The concentrations of added electrolytes, $CaCl_2$ and NaOH, are relatively low as compared to the total solutions' ionic strength, and their effect on the values of N_{agg} is relatively weak.

Another way to estimate the micelle aggregation number is to assume that the radius of the micelle hydrocarbon core, R, is equal to the length of the extended surfactant tail, l, and to divide the volume of micelle hydrocarbon core to the volume of a single tail [59]:

$$N_{max} = \frac{4\pi l^3}{3v}\ ,\ \ v = (27.4 + 26.9n) \times 10^{-3}\ \text{nm}^3 \qquad (6)$$

Here, the volume of the surfactant tail, v, and its extended tail, l, are estimated by using the Tanford formulas [43,59]: see Eq. (6) for v and Eq. (4) for l. The aggregation number determined from Eq. (6) is denoted N_{max}. In reality $R \le l$, so that $N_{agg} \le N_{max}$ for a *spherical* micelle. (For elongated ellipsoidal micelles we could have $N_{agg} > N_{max}$.)

As seen in Table 1, for C12-SME we have $N_{agg} \approx N_{max}$ in the framework of the experimental accuracy. In other words, in the micelles of C12-SME a part of the surfactant tails are completely extended, so that $R \approx l$. In contrast, for C14- and C16-SME N_{agg} is markedly smaller than N_{max}, i.e. the surfactant chains in the micelle are not completely extended. This could be due to a gain of chain-conformational free energy [60,61].

It should be also noted that the obtained values of N_{agg} for spherical micelles from Cn-SME (without additives; see Table 1) comply very well with a straight line:

$$N_{agg} = 7.75n - 3.72,\quad n = 12, 14, 16 \qquad (7)$$

The slope of this dependence, 7.75 ± 0.14, indicates that N_{agg} increases with ca. eight molecules upon the addition of one CH_2 group to the hydrocarbon tail of Cn-SME. The values of aggregation number extrapolated from Eq. (7) for n = 10 and 18 are N_{agg} = 40 and 102, respectively.

4.2. Verification of the theoretical model

The experimental values of the final equilibrium thickness of the film h_0 in Table 1 give the possibility for an independent verification of the theoretical model, which has been already used to calculate N_{agg}, φ and α. Using the values of the latter three quantities, determined as explained in Appendix B, we can apply the thin-liquid-film theory from Refs. [25,28] (which accounts for the presence of ionic micelles in the bulk) to calculate h_0. If the theoretical values of h_0 obtained in this way coincide with the experimental values of h_0, this would confirm the correctness of the used theoretical model and the values of N_{agg}, φ and α given in Table 1.

The theoretical calculation of h_0 is based on the force balance at the surfaces of the liquid film, which states that the disjoining pressure of the film should counterbalance the external capillary pressure (the sucking pressure applied in the SE cell), P_c:

$$\Pi_{el}(h_0) + \Pi_{vw}(h_0) = P_c \quad (8)$$

Here, Π_{el} and Π_{vw} are the electrostatic and van der Waals components of disjoining pressure. The capillary pressure can be easily estimated [32], $P_c \approx 2\sigma/R_{in}$, where $R_{in} = 1.5$ mm is the inner radius of the SE cell, and σ is the surface tension of the solution; see Refs. [21,22]. The dependences of Π_{el} and Π_{vw} on h_0 can be described by formulas given in Ref. [25]. In particular, Π_{el} depends on c_1, c_{mic}, α, and N_{agg}, which have been determined in Appendix B; see also Appendix C. The reason for this dependence is the fact that the counterions, which are dissociated from the micelles of the ionic surfactant in the bulk, have to be taken into account when calculating the electrostatic component of disjoining pressure. As known, Π_{el} equals the difference between the osmotic pressures of all ions in the midplane of the thin film and in the bulk; see Refs. [25,28] for details. We recall that the film of thickness h_0 does not contain surfactant micelles.

Substituting the theoretical expressions for $\Pi_{el}(h_0)$ and $\Pi_{vw}(h_0)$ in Eq. (8) and solving it numerically, we determine h_0 for each given C_S. The full system of equations and the principles of the computational procedure are described in Appendix C.

The lines in Fig. 8 present the theoretical dependencies of h_0 on C_S for C12- and C14-SME with 0 and 10 mM NaOH, calculated without using any adjustable parameters. Similar results for C16-SME are shown in Fig. 6. In Fig. 8, the two curves for the case with 10 mM NaOH correspond to smaller h_0 because the ionic strength is higher in this case, which leads to a stronger suppression of the electrostatic repulsion between the two film surfaces. The symbols in Fig. 8 correspond to the values of h_0 in Table 1. The excellent agreement between the experimental points and the theoretical curves in Fig. 8 for C12- and C14-SME and in Fig. 6 for C16-SME confirms the validity of the used theoretical model and represents a strong argument in favor of the correctness of the calculated N_{agg}, φ and α values in Table 1.

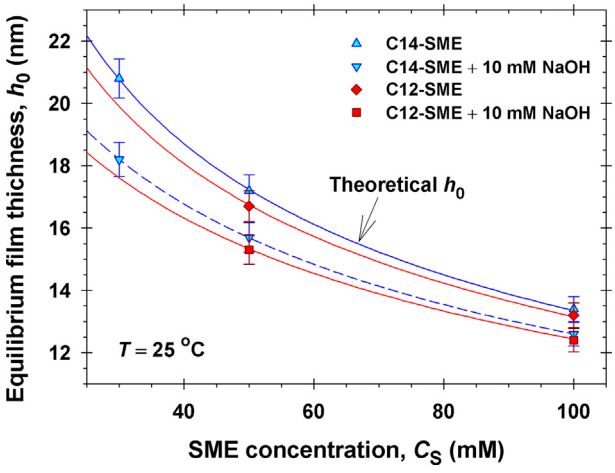

Fig. 8. Dependence of the final equilibrium thickness of the foam film on the total surfactant concentration, C_S. The symbols represent experimental values of h_0 from Table 1. The curves are the theoretical dependencies of h_0 on C_S, calculated without using any adjustable parameters.

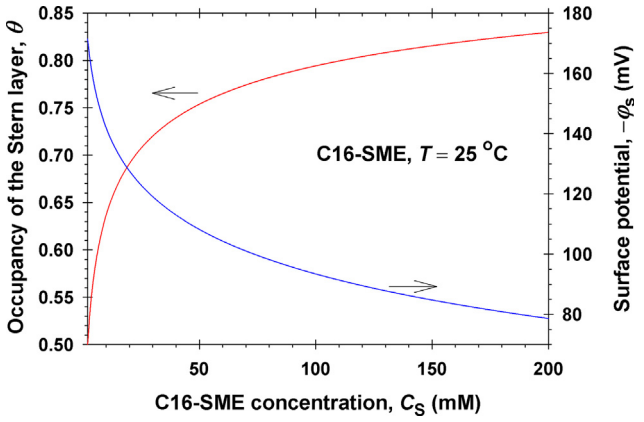

Fig. 9. Calculated surface potential, φ_s, and occupancy of the Stern layer by bound Na^+ counterions, θ, vs. C_S for the equilibrium film of thickness h_0 stabilized by C16-SME.

The calculations of the dependencies of h_0 on C_S in Appendix C include also calculation of the electric potential φ_s of the film surfaces and the occupancy of the Stern layers at the film surfaces with bound counterions, θ. (It should be noted that $\theta = 1 - \alpha_s$, where α_s is the ionization degree of the film surfaces.) As an example, the calculated dependencies of φ_s and θ on the total surfactant concentration C_S are shown in Fig. 9 for the case of C16-SME. As seen in the figure, the magnitude of the surface potential φ_s markedly decreases from 172 mV at $C_S = 2$ mM (just above the CMC) to 93 mM at $C_S = 100$ mM (the latter value being close to the micelle potential $\varphi = 92$ mV at $C_S = 100$ mM; see Table 1). This decrease of φ_s is accompanied with an increase of the occupancy of the Stern layer from $\theta = 0.50$ at $C_S = 2$ mM to $\theta = 0.79$ at $C_S = 100$ mM. Hence, the decrease of h_0 with the rise of C_S (Figs. 6 and 8) is related not only to the increased Debye screening in the diffuse electric double layer inside the film, but also to the increase of counterion binding to the film surfaces.

4.3. Micellar packing parameter and area per headgroup

The formation of micellar aggregates of different shape is related to the geometrical packing parameter, which can be estimated as follows [59]:

$$p = \frac{v}{al} \quad (9)$$

where v is the volume of the hydrophobic chain of a surfactant molecule, l is its extended length and a is the area per headgroup at the surface of micelle hydrocarbon core. It should be noted that the exact definition of p contains the radius of micelle hydrocarbon core, R, instead of the length of the extended chain, l. Here, the assumption $R \approx l$ was used as an approximation. In reality, $R \leq l$ and the value of R can be determined by minimization of micelle free energy; see e.g. Ref. [61]. The values of l and v calculated from Tanford [43] formulas, Eqs. (4) and (6), are given in Table 2.

In Table 2, a_c 0.37 nm^2 is the area per molecule in a closely packed adsorption layer, which was determined from the adsorption isotherms of Cn-SME at the air/water interface [22]. The values of the packing parameter, p_c, are calculated from Eq. (9) with $a = a_c$.

Table 2
Geometrical parameters of C*n*-SME molecules and micellar packing parameter.

Surfactant	v (nm^3)	l (nm)	a_c (nm^3)	a (nm^3) (spherical micelle)	p_c
C12-SME	0.350	1.672	0.37	0.628	0.566
C14-SME	0.404	1.925	0.37	0.629	0.567
C16-SME	0.458	2.178	0.37	0.630	0.568

We recall that $p = 1/3$, $1/2$ and 1 for spherical, cylindrical and lamellar micelles, respectively. The values of p_c correspond to the packing parameter of hypothetical C*n*-SME micelles, for which the electrostatic repulsion between the headgroups is completely switched off. The obtained values of p_c, which are slightly above 0.5, indicate that C*n*-SME could form wormlike micelles at sufficiently high concentrations of added electrolyte.

At not so high ionic strengths, the electrostatic repulsion between the surfactant headgroups is significant and promotes the formation of spherical micelles, as indicated by the film-stratification experiments described above. For spherical micelles $p = 1/3$ [59,61]. Then, using Eq. (9) and the values of v and l in Table 2 one can calculate the area per surfactant molecule, a, at the surface of a spherical micelle. As seen in Table 2, the values of a estimated in this way are with more than 50% greater than the area a_c per surfactant molecule in a closely packed monolayer.

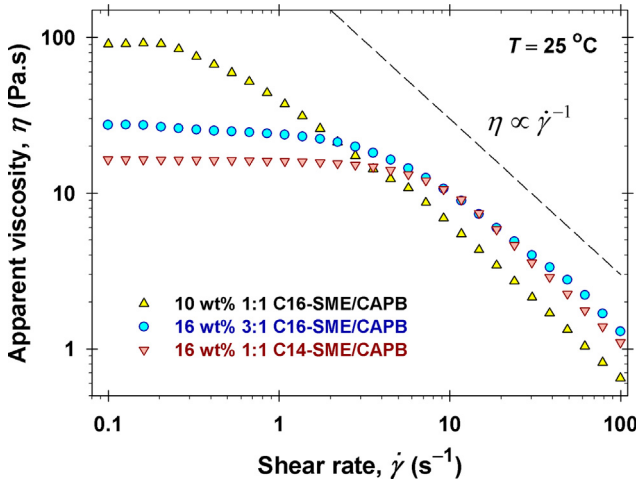

Fig. 10. Plots of experimental data for the apparent viscosity, η, vs. the shear rate $\dot{\gamma}$ for mixed micellar solutions of C*n*-SME and CAPB at different total surfactant concentrations and weight ratios of the two surfactants. The dashed line corresponds to $\eta \propto \dot{\gamma}^{-1}$.

5. Micelle growth in mixed solutions of C*n*-SME and CAPB

In a previous study [22] it was shown that the CMC of mixed solutions of C*n*-SME and CAPB obeys the law of ideal mixing. Here, we extend this analysis to concentrated solutions of C*n*-SME and CAPB to investigate whether the mixing of these two surfactants gives rise to the growth of giant micelles, as this has been observed with mixed solutions of other anionic surfactants with CAPB [45–47,62,63]. The growth of such micelles is usually detected as a considerable increase of solution's viscosity, from 10^2 to 10^6 times the viscosity of water. Most frequently, this rise of viscosity is due to the formation of long and entangled wormlike micelles that can be proved by cryogenic transmission electron microscopy (cryo-TEM) [45,46].

In our experiments, we mixed C*n*-SME and CAPB ($n = 14$, 16) at different weight ratios. At sufficiently high concentrations, an increase of viscosity by orders of magnitude was detected by the rotational rheometer (see Section 2.2). As an illustration, Fig. 10 shows typical data from steady shear measurements of the apparent viscosity η vs. the shear rate $\dot{\gamma}$. One sees that the solutions exhibit non-Newtonian behavior. At low values of $\dot{\gamma}$, a plateau is observed, which defines the zero-shear viscosity, η_0. At higher values of $\dot{\gamma}$, we observe shear thinning with linear dependence of η on $\dot{\gamma}^{-1}$. Such rheological behavior is typical for wormlike micelles, but could be observed also with branched multi-connected micelles; see e.g. Ref. [45].

Fig. 11 summarizes the results of our systematic rheological measurements with mixed solutions of C14- and C16-SME with CAPB. One sees that η_0 increases with the rise of the total surfactant concentration and of the fraction of CAPB in the mixture. Under the same conditions, the solutions with C16-SME are more viscous than those with C14-SME.

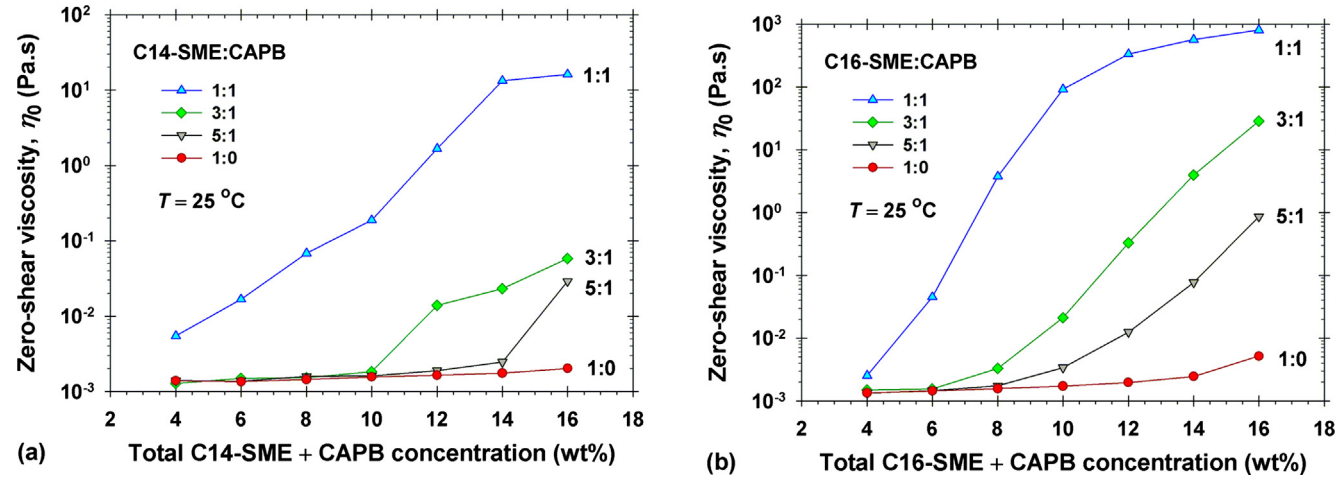

Fig. 11. Plots of experimental data for the zero-shear viscosity, η_0, vs. the total surfactant concentration for mixed solutions of C*n*-SME and CAPB at four different weight ratios of these two surfactants shown in the figure: (a) C14-SME + CAPB; (b) C16-SME + CAPB.

The solutions of C*n*-SME alone (denoted with 1:0 in Fig. 11) exhibit Newtonian behavior. At a concentration of 16 wt%, their viscosity is 2.0 mPa·s for C14-SME and 5.2 mPa·s for C16-SME.

In this series of experiments, the maximal viscosities have been measures at 1:1 C*n*-SME/CAPB (Fig. 11). At total surfactant concentration of 16 wt%, the zero-shear viscosity is η_0 = 16 Pa·s for C14-SME and η_0 = 810 Pa·s for C16-SME.

Note that the data in Fig. 11 refer to the viscosity of mixed solutions of C*n*-SME and CAPB without any additives. In view of Refs. [18,45–47,63], one could expect that the addition of NaCl or cosurfactants (e.g. fatty acids and/or fragrances) one could additionally increase the viscosity of the mixed C*n*-SME + CAPB solutions, and especially of those with lower content of CAPB. It should be noted that CAPB itself contains admixture of NaCl. Thus, 1 wt% CAPB contains 0.164 wt% NaCl, which is 28 mM NaCl. However, this amount of NaCl is relatively small. Typically, NaCl is used as thickening agent at concentrations in the range of 100–1000 mM [18]. Hence, the large values of η_0 in Fig. 11 are mostly due to the synergism of C*n*-SME and CAPB with respect to the micelle growth, rather than to the presence of NaCl admixture in CAPB.

The typical viscosity of a shampoo formulation is of the order of 5 Pa·s. Hence, the data in Fig. 11 indicate that C14- and C16-SME in mixture with CAPB represent a promising system for formulations in personal-care and house-hold detergency. The structure of the formed micelles and the effect of various additives/cosurfactants could be a subject for subsequent studies.

6. Conclusions

The present paper is the first systematic study on stratifying films from solutions of sulfonated methyl esters, C*n*-SME, n = 12, 14, 16, and on the properties of their micelles, such as aggregation number, N_{agg}, surface electric potential, φ, and ionization degree, α. The effects of surfactant concentration and chainlength, as well as of added $CaCl_2$ and NaOH on these micellar properties are investigated. Following the method developed in Refs. [25,28], we determined N_{agg}, φ, and α, by theoretical analysis of the data for stratifying films (Table 1). For the accurate determination of N_{agg}, we calculated the variation of the monomer concentration, c_1, using the detailed micellization model from Ref. [58]. The results show that in the concentration range between 30 and 100 mM C*n*-SME, spherical micelles are formed with aggregation number increasing with the surfactant concentration and chainlength in the range of 56–59 for C12-SME; 66–73 for C14-SME, and 78–87 for C16-SME. The addition of 2.4 mM $CaCl_2$ (as in hard water) does not produce a significant effect on the micellar properties, in agreement with the fact that the SMEs are among the surfactants of the lowest hard-water sensitivity [7,64,65].

As an independent verification of the model used to interpret the thin-film data, we compared the theoretically calculated and experimentally measured equilibrium film thickness, h_0. The obtained excellent agreement between theory and experiment without using any adjustable parameters (Figs. 6 and 8) is a strong argument in favor of the correctness of the used model and the determined values of N_{agg}, φ and α.

Furthermore, in contrast with a previous finding [22] that the mixed solutions of SME and CAPB exhibit ideal mixing with respect to the CMC values, we established that these two surfactants exhibit a strong synergism with respect to the micelle growth at higher surfactant concentrations. The obtained high values of the zero-shear viscosity, up to 810 Pa·s, indicate the growth of giant mixed micelles, most probably wormlike, like those observed in the mixed solutions of other anionic surfactants with CAPB [45,46]. To the best of our knowledge, this is the first study where synergistic rise of viscosity is reported for mixed solutions of C*n*-SME with a zwitterionic surfactant. These results imply that the mixed solutions of SME and CAPB represent a promising system for formulations in personal-care and house-hold detergency, having in mind also the other useful properties of SME, such as high hard water tolerance, biodegradability and skin compatibility. For example, C*n*-SMEs could serve as substituents of sodium laureth sulfates (SLES) in shampoo formulations.

An interesting continuation of this study would be to investigate both experimentally and theoretically the reasons for the strong synergism with respect to micelle growth in the mixed C*n*-SME – CAPB solutions and to reveal which component of the micellar free energy is responsible for the observed effects.

Acknowledgements

The authors gratefully acknowledge the support from KL-Kepong Oleomas, Malaysia; from the Horizon 2020 project ID: 692146-H2020-EU.4.b "Materials Networking", and from project BG05M2OP001-1.002-0023 of the Operational Programme "Science and Education for Smart Growth", Bulgaria.

Appendix A. Supplementary material

Supplementary data to this article can be found online at https://doi.org/10.1016/j.jcis.2018.12.034.

References

[1] L. Cohen, F. Soto, M.S. Luna, Separation and extraction of Φ-methyl ester sulfoxylates: new features, J. Surf. Deterg. 4 (2001) 73–74.
[2] Z.A. Maurad, R. Ghazali, P. Siwayanan, Z. Ismail, S. Ahmad, Alpha-sulfonated methyl ester as an active ingredient in palm-based powder detergents, J. Surf. Deterg. 9 (2006) 161–167.
[3] S. Ahmad, P. Siwayanan, Z.A. Maurad, H.A. Aziz, H.S. Soi, Methyl esters as a route for the production of surfactant feedstocks, Inform 18 (2007) 216–228.
[4] D. Martinez, G. Orozco, S. Rincón, I. Gil, Simulation and pre-feasibility analysis of the production process of α-methyl ester sulfonates (α-MES), Bioresource Technol. 101 (2010) 8762–8771.
[5] I. Johansson, M. Swensson, Surfactant based on fatty acids and other natural hydrophobes, Curr. Opin. Coll. Int. Sci. 6 (2001) 178–188.
[6] L. Cohen, F. Soto, A. Melgarejo, D.W. Roberts, Performance of Φ-sulfo fatty methyl ester sulfonate versus linear alkylbenzene sulfonate, secondary alkane sulfonate and α-sulfo fatty methyl ester sulfonate, J. Surf. Deterg. 11 (2008) 181–186.
[7] R. Ghazali, Z.A. Maurad, P. Siwayanan, M. Yusof, S. Ahmad, Assessment of aquatic effects of palm-based alpha-sulfonated methyl ester (SME), J. Oil Palm Res. 18 (2006) 225–230.
[8] R. Ghazali, S. Ahmad, Biodegradability and ecotoxicity of palm stearin-based methyl ester sulfonates, J. Oil Palm Res. 16 (2004) 39–44.
[9] P. Siwayanan, R. Aziz, N.A. Bakar, H. Ya, R. Jokiman, S. Chelliapan, Characterization of phosphate-free detergent powders incorporated with palm C16 methyl ester sulfonate (C16MES) and linear alkyl benzene sulfonic acid (LABSA), J. Surf. Deterg. 17 (2014) 871–880.
[10] P. Siwayanan, R. Aziz, N.A. Bakar, H. Ya, R. Jokiman, S. Chelliapan, Detergency stability and particle characterization of phosphate-free spray dried detergent powders incorporated with palm C16 methyl ester sulfonate (C16MES), J. Oleo Sci. 63 (2014) 585–592.
[11] Y.S. Lim, R.D. Stanimirova, H. Xu, J.T. Petkov, Sulfonated methyl ester a promising surfactant for detergency in hard water conditions, H&PC Today 11 (2016) 47–51.
[12] A.J. Stirton, R.G. Bistline, J.K. Weil, W.C. Ault, E.W. Maurer, Sodium salts of alkyl esters of α-sulfo fatty acid. Wetting, lime soap dispersion, and related properties, JAOCS 39 (1962) 128–131.
[13] A.J. Stirton, α-sulfo fatty acids and derivatives. Synthesis, properties and use, JAOCS 39 (1962) 490–496.
[14] M. Fujiwara, T. Okano, T.-H. Nakashima, A.A. Nakamura, G. Sugihara, A temperature study on critical micellization concentration (CMC), solubility, and degree of counterion binding of α-sulfonatomyristic acid methyl ester in water by electroconductivity measurements, Colloid Polym. Sci. 275 (1997) 474–479.
[15] S.R. Patil, T. Mukaiyama, A.K. Rakshit, α-sulfonato palmitic acid methyl ester-hexaoxyethylene monododecyl ether mixed surfactant system: interfacial, thermodynamic, and performance property study, J. Surf. Deterg. 7 (1) (2004) 87–96.
[16] W.H. Lim, R.A. Ramle, The behavior of methyl esters sulfonate at the water-oil interface: straight-chained methyl ester from lauryl to stearyl as an oil phase, J. Dispersion Sci. Technol. 30 (1) (2009) 131–136.

[17] S.P. Wong, W.H. Lim, S.F. Cheng, C.H. Chuan, Physico-chemical properties of mixed anionic/cationic surfactant solution: mixtures of sodium laurate methyl ester α-sulphonate and tetradecyltrimethylammonium bromide, J. Oil Palm Res. 23 (April) (2011) 968–973.
[18] M. Luo, Z. Jia, H. Sun, L. Liao, Q. Wen, Rheological behavior and microstructure of an anionic surfactant micelle solution with pyroelectric nanoparticle, Colloids Surf. A 395 (2012) 267–275.
[19] S.P. Wong, W.H. Lim, S.-F. Cheng, C.H. Chuan, Properties of sodium methyl ester alpha-sulfo alkylate/trimethylammonium bromide mixtures, J. Surf. Deterg. 15 (5) (2012) 601–611.
[20] H. Xu, P. Li, K. Ma, R.J.L. Welbourne, J. Penfold, D.W. Roberts, R.K. Thomas, J.T. Petkov, Adsorption of methyl ester sulfonate at the air-water interface: can limitations of the application of the Gibbs equation be overcome by computer purification?, Langmuir 33 (38) (2017) 9944–9953
[21] K.D. Danov, R.D. Stanimirova, P.A. Kralchevsky, E.S. Basheva, V.I. Ivanova, J.T. Petkov, Sulfonated methyl esters of fatty acids in aqueous solutions: interfacial and micellar properties, J. Colloid Interface Sci. 457 (2015) 307–318.
[22] V.I. Ivanova, R.D. Stanimirova, K.D. Danov, P.A. Kralchevsky, J.T. Petkov, Sulfonated methyl esters, linear alkylbenzene sulfonates and their mixed solutions: micellization and effect of Ca^{2+} ions, Colloids Surf. A 519 (2017) 87–97.
[23] H. Xu, R.K. Thomas, J. Penfold, P.X. Li, K. Ma, R.J.L. Welbourne, D.W. Roberts, J.T. Petkov, The impact of electrolyte on the adsorption of anionic surfactant methyl ester sulfonate at the air-water solution interface: surface multilayer formation, J. Colloid Interface Sci. 512 (2018) 231–238.
[24] H. Xu, P. Li, K. Ma, R.J.L. Welbourne, J. Doutch, J. Penfold, R.K. Thomas, D.W. Roberts, J.T. Petkov, K.L. Choo, S.Y. Khoo, Adsorption and self-assembly in methyl ester sulfonate surfactants, their eutectic mixtures and the role of electrolytes, J. Colloid Interface Sci. 516 (2018) 456–465.
[25] S.E. Anachkov, K.D. Danov, E.S. Basheva, P.A. Kralchevsky, K.P. Ananthapadmanabhan, Determination of the aggregation number and charge of ionic micelles from the stepwise thinning of foam films, Adv. Colloid Interface Sci. 183–184 (2012) 55–67.
[26] E.S. Basheva, P.A. Kralchevsky, K.D. Danov, K.P. Ananthapadmanabhan, A. Lips, The colloid structural forces as a tool for particle characterization and control of dispersion stability, Phys. Chem. Chem. Phys. 9 (2007) 5183–5198.
[27] D. Wasan, A. Nikolov, Thin liquid films containing micelles or nanoparticles, Curr. Opin. Coll. Int. Sci. 13 (2008) 128–133.
[28] K.D. Danov, E.S. Basheva, P.A. Kralchevsky, K.P. Ananthapadmanabhan, A. Lips, The metastable state of foam films containing electrically charged micelles or particles: experiment and quantitative interpretation, Adv. Colloid Interface Sci. 168 (2011) 50–70.
[29] P.A. Kralchevsky, N.D. Denkov, Analytical expression for the oscillatory structural surface force, Chem. Phys. Lett. 240 (1995) 385–392.
[30] E. Mileva, D. Exerowa, Amphiphilic nanostructures in foam films, Curr. Opin. Colloid Interface Sci. 13 (2008) 120–127.
[31] A.D. Nikolov, D.T. Wasan, P.A. Kralchevsky, I.B. Ivanov, Ordered structures in thinning micellar foam and latex films, in: N. Ise, I. Sogami (Eds.), Ordering and Organization in Ionic Solutions, World Scientific Co., Singapore, 1988, pp. 302–314.
[32] A.D. Nikolov, D.T. Wasan, Ordered micelle structuring in thin films from anionic surfactant solutions: I. Experimental, J. Colloid Interface Sci. 133 (1989) 1–12.
[33] A.D. Nikolov, P.A. Kralchevsky, I.B. Ivanov, D.T. Wasan, Ordered micelle structuring in thin films formed from anionic surfactant solutions: II. Model development, J. Colloid Interface Sci. 133 (1989) 13–22.
[34] N.D. Denkov, H. Yoshimura, K. Nagayama, Nanoparticle arrays in freely suspended vitrified films, Phys. Rev. Lett. 76 (1996) 2354–2357.
[35] N.D. Denkov, H. Yoshimura, K. Nagayama, Method for controlled formation of vitrified films for cryo-electron microscopy, Ultramicroscopy 65 (1996) 147–158.
[36] T. Satsuki, K. Umehara, Y. Yoneyama, Performance and physicochemical properties of α-sulfo fatty acid methyl esters, JAOCS 69 (1992) 672–677.
[37] A. Scheludko, D. Exerowa, Device for interferometric measuring of the thickness of microscopic foam films, C.R. Acad. Bulg. Sci. 7 (1959) 123–132.
[38] A. Sheludko, Thin liquid films, Adv. Colloid Interface Sci. 1 (1967) 391–464.
[39] I.U. Vakarelski, R. Manica, E.Q. Li, E.S. Basheva, D.Y.C. Chan, S.T. Thoroddsen, Coalescence dynamics of mobile and immobile fluid interfaces, Langmuir 34 (2018) 2096–2108.
[40] O.D. Velev, T.D. Gurkov, I.B. Ivanov, R.P. Borwankar, Abnormal thickness and stability of nonequilibrium liquid films, Phys. Rev. Lett. 75 (1995) 264–267.
[41] V. Bergeron, C.J. Radke, Equilibrium measurements of oscillatory disjoining pressure in aqueous foam films, Langmuir 8 (1992) 3020–3026.
[42] R.C. Kootiani, A.B. Samsuri, Measurements of the thickness of thin foam films by laser interferometry, Int. J. Modern Eng. Res. 3 (2013) 3673–3679.
[43] C. Tanford, The Hydrophobic Effect. The Formation of Micelles and Biological Membranes, 2nd edition,., Wiley, New York, 1980.
[44] X. Tang, W. Zou, P.H. Koenig, S.D. McConaughy, M.R. Weaver, D.M. Eike, M.J. Schmidt, R.G. Larson, Multiscale modelling of the effect of salt and perfume raw materials on the rheological properties of commercial threadlike micellar solutions, J. Phys. Chem. B 121 (2017) 2468–2485.
[45] G.S. Georgieva, S.E. Anachkov, I. Lieberwirth, K. Koynov, P.A. Kralchevsky, Synergistic growth of giant wormlike micelles in ternary mixed surfactant solutions: effect of octanoic acid, Langmuir 32 (2016) 12885–12893.
[46] S.E. Anachkov, G.S. Georgieva, L. Abezgauz, D. Danino, P.A. Kralchevsky, Viscosity peak due to shape transition from wormlike to disklike micelles: effect of dodecanoic acid, Langmuir 34 (2018) 4897–4907.
[47] Z. Mitrinova, S. Tcholakova, N. Denkov, Control of surfactant solution rheology using medium-chain cosurfactants, Colloids Surf. A 538 (2018) 173–184.
[48] P.A. Kralchevsky, A.D. Nikolov, D.T. Wasan, I.B. Ivanov, Formation and expansion of dark spots in stratifying foam films, Langmuir 6 (1990) 1180–1189.
[49] I.B. Ivanov, K.D. Danov, K.P. Ananthapadmanabhan, A. Lips, Interfacial rheology of adsorbed layers with surface reaction: on the origin of the dilatational surface rheology, Adv. Colloid Interface Sci. 114–115 (2005) 61–92.
[50] M. Piech, J.Y. Walz, The structuring of nonadsorbed nanoparticles and polyelectrolyte chains in the gap between a colloidal particle and plate, J. Phys. Chem. B 108 (2004) 9177–9188.
[51] S.H.L. Klapp, Y. Zeng, D. Qu, R. von Klitzing, Surviving structure in colloidal suspensions squeezed from 3D to 2D, Phys. Rev. Lett. 100 (2008) 118303.
[52] S. Grandner, Y. Zeng, R. von Klitzing, S.H.L. Klapp, Impact of surface charges on the solvation forces in confined colloidal solutions, J. Chem. Phys. 131 (2009) 154702.
[53] S.H.L. Klapp, S. Grandner, Y. Zeng, R. von Klitzing, Charged silica suspensions as model materials for liquids in confined geometries, Soft Matter 6 (2010) 2330–2336.
[54] Y. Zeng, S. Grandner, C.L.P. Oliveira, A.F. Thünemann, O. Paris, R. von Klitzing, Effect of particle size and Debye length on order parameters of colloidal silica suspensions under confinement, Soft Matter 7 (2011) 10899–10909.
[55] B. Jönsson, A. Broukhno, J. Forsman, T. Åkesson, Depletion and structural forces in confined electrolyte solutions, Langmuir 19 (2003) 9914–9922.
[56] D. Qu, G. Brotons, V. Bosio, A. Fery, T. Salditt, D. Langevin, R. von Klitzing, Interactions across liquid thin films, Colloids Surf. A 303 (2007) 97–109.
[57] R. von Klitzing, E. Thormann, T. Nylander, D. Langevin, C. Stubenrauch, Confinement of linear polymers, surfactants, and particles between interfaces, Adv. Colloid Interface Sci. 155 (2010) 19–31.
[58] K.D. Danov, P.A. Kralchevsky, K.P. Ananthapadmanabhan, Micelle-monomer equilibria of ionic surfactants and in ionic-nonionic mixtures: a generalized phase separation model, Adv. Colloid Interface Sci. 206 (2014) 17–45.
[59] J. Israelachvili, Intermolecular and Surface Forces, 3rd edition., Academic Press, 2011.
[60] A.N. Semenov, Contribution to the theory of microphase layering in blockcopolymer melts, Sov. Phys. JETP 61 (1985) 733–742.
[61] K.D. Danov, P.A. Kralchevsky, S.D. Stoyanov, J.L. Cook, I.P. Stott, E.G. Pelan, Growth of wormlike micelles in nonionic surfactant solutions: quantitative theory vs. experiment, Adv. Colloid Interface Sci. 256 (2018) 1–22.
[62] N.C. Christov, N.D. Denkov, P.A. Kralchevsky, K.P. Ananthapadmanabhan, Synergistic sphere-to-rod micelle transition in mixed solutions of sodium dodecyl sulfate and cocoamidopropyl betaine, A. Lips, Langmuir 20 (2004) 565–571.
[63] Z. Mitrinova, S. Tcholakova, K. Golemanov, N. Denkov, M. Vethamuthu, K.P. Ananthapadmanabhan, Surface and foam properties of SLES + CAPB + fatty acid mixtures: Effect of pH for C12–C16 acids, Colloids Surf. A 438 (2013) 186–198.
[64] L. Cohen, F. Trujillo, Performance of sulfoxylated fatty acid methyl esters, J. Surfact. Deterg. 2 (1999) 363–365.
[65] Y.S. Lim, N.B. Baharudin, Y.W. Ung, Methyl ester sulfonate: a high-performance surfactant capable of reducing builders dosage in detergents, J. Surfact. Deterg. (2018), https://doi.org/10.1002/jsde.12230.

Supplementary Material

for the article

Properties of the micelles of sulfonated methyl esters determined from the stepwise thinning of foam films and by rheological measurements

Elka S. Basheva[a], Krassimir D. Danov[a], Gergana M. Radulova[a], Peter A. Kralchevsky[a], Hui Xu[b], Yee Wei Ung[b], Jordan T. Petkov[b]

[a]*Department of Chemical & Pharmaceutical Engineering, Faculty of Chemistry & Pharmacy, Sofia University, 1164 Sofia, Bulgaria. E-mail: pk@lcpe.uni-sofia.bg; Fax: +359 2 9625643*

[b]*KL-Kepong Oleomas SDN BHD, Menara KLK, Jalan PJU 7/6, Mutiara Damansara, 47810 Petaling Jaya, Selangor Dalur Ehsan, Malaysia*

Appendix A. Experimental results – stepwise thinning of foam films from C*n*-SME solutions at concentrations above the CMC

Figs. A1 and A2 show the typical experimental dependencies of the film thickness, *h*, on time, *t*, obtained for foam films formed in a SE cell from micellar solutions of C12-SME and C14-SME. The used concentrations of C*n*-SME and of the additives, 10 mM NaOH or 2.4 mM $CaCl_2$, are denoted in the figures. Analogous data for C16-SME are given in Fig. 3 in the main text.

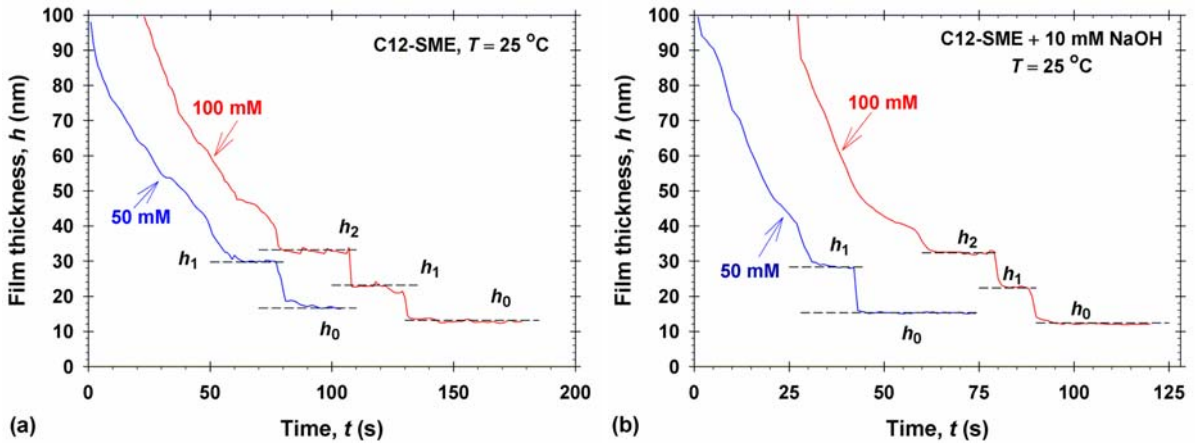

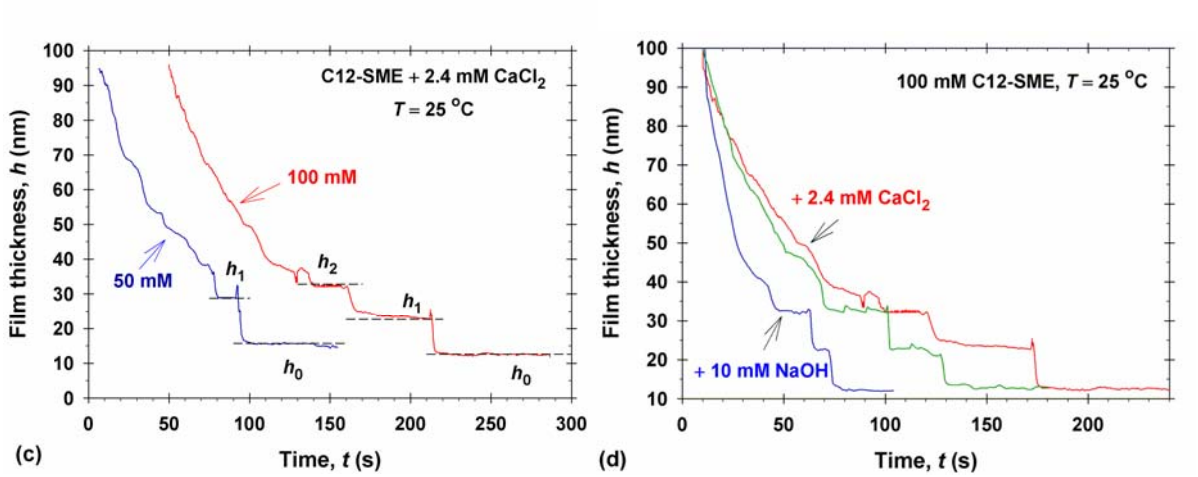

Fig. A1. Experimental dependencies of the film thickness, h, on time, t, for foam films formed in a SE cell from C12-SME solutions of concentrations denoted in the figure: (a) C12-SME alone; (b) with added 10 mM NaOH; (c) with added 2.4 mM $CaCl_2$; (d) comparison of the three drainage curves at 100 mM C12-SME.

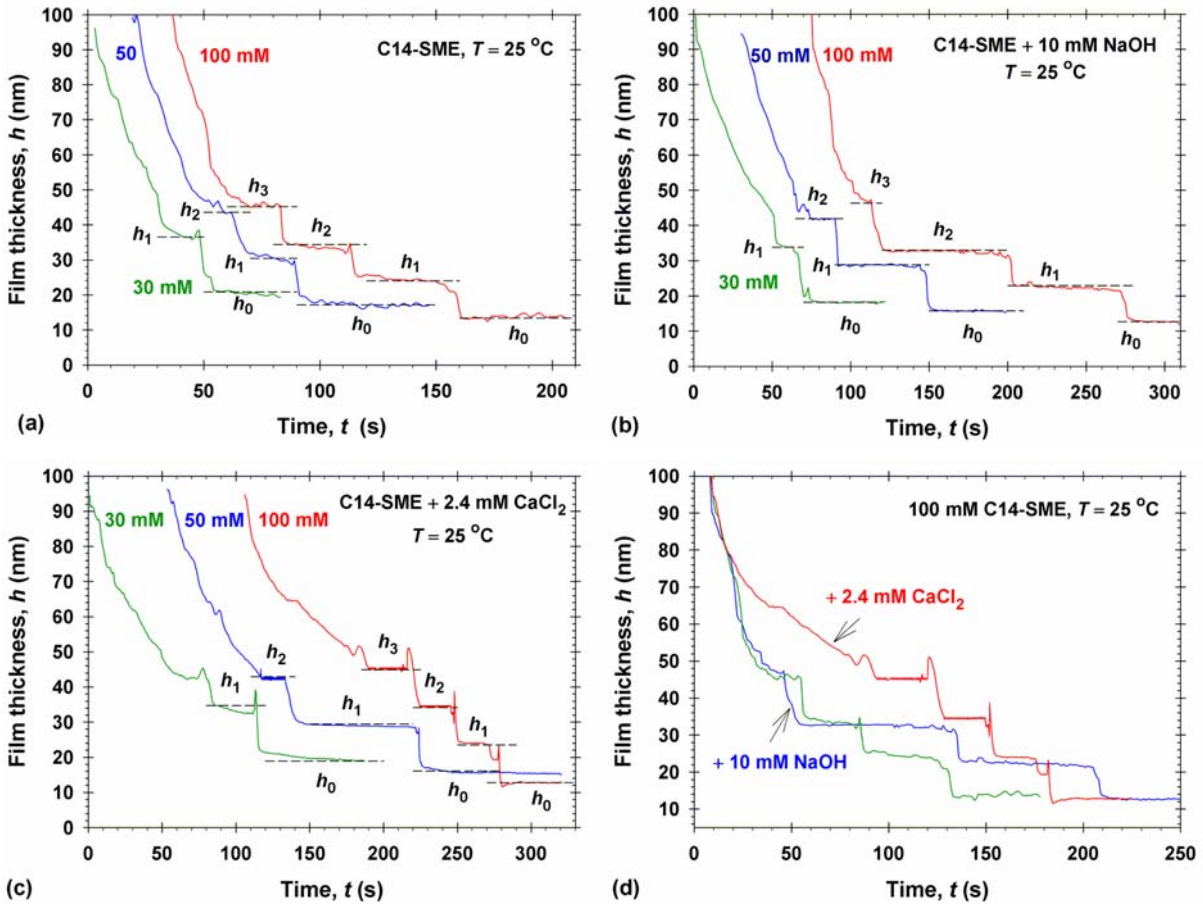

Fig. A2. Experimental dependencies of the film thickness, h, on time, t, for foam films formed in a SE cell from C14-SME solutions of concentrations denoted in the figure: (a) C14-SME alone; (b) with added 10 mM NaOH; (c) with added 2.4 mM $CaCl_2$; (d) comparison of the three drainage curves at 100 mM C14-SME.

Fig. A3 presents experimental data for the dependence of the film thickness at the steps, h_0, h_1, h_2, and h_3, on the surfactant concentration for C12-, C14- and C16-SME in the presence of 10 mM NaOH. Analogous results for C12-, C14- and C16-SME without and with added 2.4 mM $CaCl_2$ are shown in Fig. 4 of the main text.

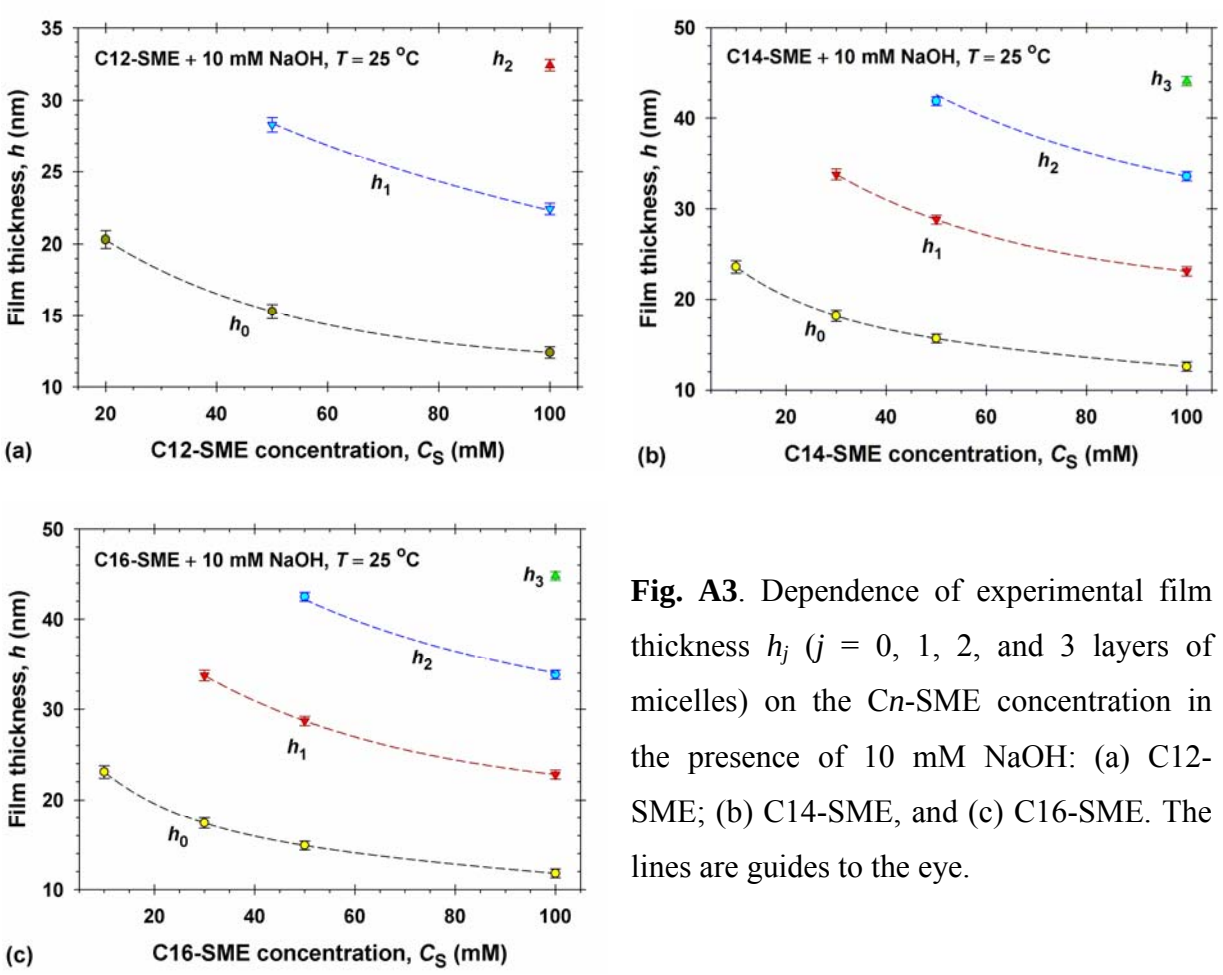

Fig. A3. Dependence of experimental film thickness h_j (j = 0, 1, 2, and 3 layers of micelles) on the Cn-SME concentration in the presence of 10 mM NaOH: (a) C12-SME; (b) C14-SME, and (c) C16-SME. The lines are guides to the eye.

Appendix B. Physicochemical model of the micelle–monomer equilibria in the investigated solutions

Here, we apply the physicochemical model for the equilibrium between micelles and monomers in mixed solutions of ionic and nonionic surfactants developed in Ref. [1].

The dimensionless surface electrostatic potential of the micelles, Φ_s, is defined to be positive and is related to the dimensional electrostatic potential, φ, as follows:

$$\Phi_s \equiv \left| \frac{e\varphi}{k_B T} \right| > 0$$

k_B is the Boltzmann constant, T is the absolute temperature, e is the elementary electric charge.

Because the used samples of SME contain small admixtures of nonionic surfactants, the presence of such admixtures is taken into account in the model. The basic equations of the model are as follows [1]:

Chemical equilibrium between monomers and micelles. The chemical equilibrium of the ionic and nonionic species is described by the equations:

$$\ln(c_1\gamma_\pm) = \ln K_1^{(\mathrm{mic})} + \ln y_1 + \Phi_s \tag{B1}$$

$$\ln c_n = \ln K_n^{(\mathrm{mic})} + \ln y_n \tag{B2}$$

where $\gamma_\pm$ is the bulk activity coefficient; c_1 and c_n are the bulk concentrations of ionic and nonionic monomers, respectively; $K_1^{(\mathrm{mic})}$ and $K_n^{(\mathrm{mic})}$ are the micellization constants of the ionic and nonionic surfactants; y_1 and y_n are the mole fractions of the molecules of ionic surfactant without bound counterions and of the nonionic surfactant in the micelles. For simplicity, the mixing of the two components in the micelles is assumed to be ideal.

The effect of counterion binding is taken into account by the equation:

$$\ln(K_{St}c_1c_2\gamma_\pm^2) = \ln K_1^{(\mathrm{mic})} + \ln y_2 \tag{B3}$$

where K_{St} is the Stern constant, c_2 is the bulk concentration of free counterions, and y_2 is the mole fraction of the ionic surfactant molecules with bound counterions in the micelles; see Eqs. (4.2) and (4.3) in Ref. [1] and the discussion therein. In addition, we have:

$$y_1 + y_2 + y_n = 1 \tag{B4}$$

Mass balance equations. Let C_S be the total concentration of the ionic surfactant; C_n – the total concentration of the nonionic surfactant; C_A – the concentration of counterions due to the added salt, and c_{mic} – the total concentration of (ionic and nonionic) surfactant molecules in micellar form. Then, the mass balance equations acquire the form:

$$c_1 + (1 - y_n)c_{mic} = C_S \tag{B5}$$

$$c_2 + y_2c_{mic} = C_S + C_A \tag{B6}$$

$$c_n + y_nc_{mic} = C_n \tag{B7}$$

Jellium model and bulk activity coefficient. For description of the micelle electrostatic potential, the most adequate is the jellium model [3]. In this model, the micelles do not contribute to the ionic strength, I, and hence

$$I = \frac{1}{2}(c_1 + c_2 + C_A) \tag{B8}$$

The activity coefficient is estimated from the semi-empirical equation:

$$\log_{10}\gamma_{\pm} = bI - \frac{AI^{1/2}}{1+Bd_iI^{1/2}} \tag{B9}$$

originating from the Debye-Hückel theory. In Eq. (B9), the empirical parameters, corresponding to NaCl at 25 ºC, are b = 0.055 M^{-1}, A = 0.5115 $M^{-1/2}$ and Bd_i = = 1.316 $M^{-1/2}$. It has been shown that these parameters can be used with a good accuracy for a wide range of surfactant solutions containing sodium counterions [3].

The Mitchell-Ninham equation assumes that the micelles are in a tension-free state, i.e. there is equilibration of the repulsive and attractive forces acting tangentially to the micelle surface. Combining the jellium model with the condition for tension free state, one arrives to the following equations [1]:

$$(1-y_n)\gamma_0 = 8\varepsilon\varepsilon_0\kappa(\frac{k_BT}{e})^2\{H\sinh^2(\frac{\Phi_s}{4}) - \frac{\Phi_s\nu}{4}\frac{\frac{\Phi_s}{4}-\tanh(\frac{\Phi_s}{4})}{H\sinh(\frac{\Phi_s}{2})} + \frac{2}{\kappa R_m}\ln[\cosh(\frac{\Phi_s}{4})]\} \tag{B10a}$$

$$H \equiv [1+\nu\frac{\sinh(\Phi_s)-\Phi_s}{\cosh(\Phi_s)-1}]^{1/2} \tag{B10b}$$

where γ_0 is the non-electrostatic component of micelle interfacial tension, ε_0 is the dielectric permittivity of vacuum, ε is the relative dielectric constant of solvent, R_m is the radius of the spherical micelles. The Debye parameter, κ, and the coefficient ν are defined as follows:

$$\kappa^2 \equiv \frac{2e^2I}{\varepsilon\varepsilon_0k_BT}\ ,\ \nu \equiv \frac{y_1c_{mic}}{2I} < 1 \tag{B10c}$$

This physicochemical model has been used to determine the critical micelle concentration (CMC) and the dependence of CMC on the concentrations of added salt and of the nonionic admixture [1,2]. The model is valid also at concentrations above the CMC and describes the concentrations of ionic and nonionic monomers; the concentration of free counterions; the electrostatic potentials of the micelles, and the degree of micelle ionization, α.

Table B1. Micellar parameters for C*n*-SME and for the nonionic admixture [2].

N	γ_0 (mN/m)	K_{St} (M^{-1})	$K_l^{(mic)}$ (M)	$K_n^{(mic)}$ (M)
12	3.67	2.86	6.43×10^{-4}	5.94×10^{-6}
14	3.65	2.86	6.64×10^{-5}	6.30×10^{-7}
16	3.63	2.86	7.14×10^{-6}	5.71×10^{-8}

Table B1 contains the values of the micellar constants, $K_1^{(mic)}$ and $K_n^{(mic)}$, the Stern constant, K_{St}, and the micelle interfacial tension, γ_0, obtained by processing of experimental data for the CMCs of C*n*-SME in Ref. [2].

The principles of the computational procedure are as follows. The input parameters are the three experimental concentrations, C_S, C_A and C_n,, and the four micellar parameters in Table B1, viz. γ_0, K_{St}, $K_1^{(mic)}$, and $K_n^{(mic)}$. Equations (B1)–(B10) form a system of ten equations for determining the ten unknown quantities, viz. c_1, c_2, c_n, c_{mic}, y_1, y_2, y_n, Φ_s, I and $\gamma_\pm$. The computational procedure for solving this mathematical problem is very similar to that described in Ref. [1].

In Fig. 6 of the paper and in Fig. B1, we have plotted the calculated dependences of c_1 on the total surfactant concentration, C_S, for different mol% of the nonionic admixture relative to the main anionic surfactant. The calculations are performed for solutions without added salts or NaOH. One sees that at molar fractions of the nonionic surfactant, which are close to (or larger than) the fractions of the real nonionic admixtures, their effect on c_1 is negligibly small. In the value of C_A we have taken into account the admixture of NaCl in the used batches of C*n*-SME determined by electric conductivity measurements [2].

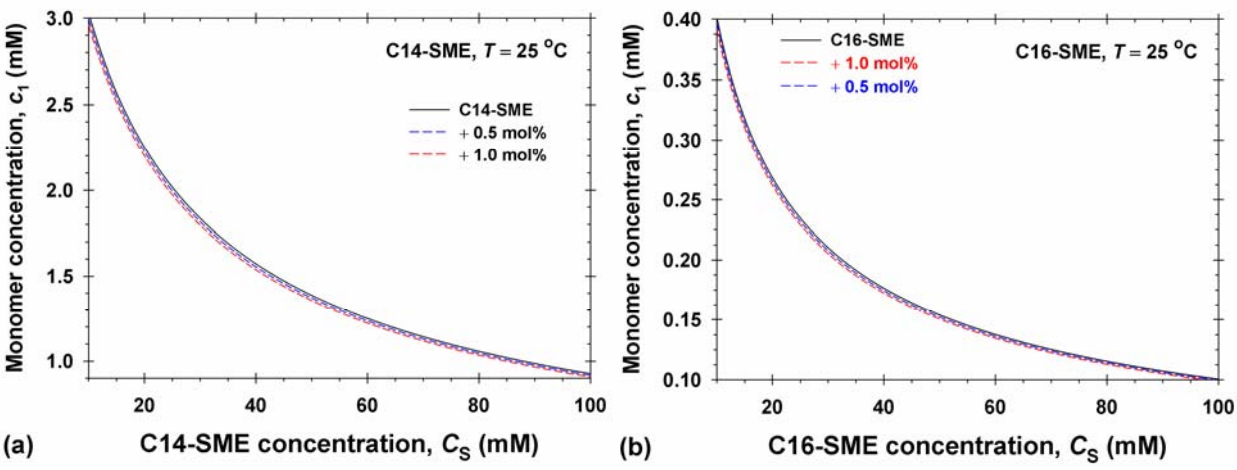

Fig. B1. Calculated bulk concentration of surfactant monomers, c_1, as a function of the total C*n*-SME concentration, C_S, above the CMC for different mol% of nonionic admixture (C*n* unsulfonated methyl ester): (a) C14-SME; (b) C16-SME.

In the case of added $CaCl_2$, the values of c_1, φ and α in Table 1 in the main text have been determined using an extended model, which takes into account the presence of both Na^+ and Ca^{2+} ions [1]. We have used the value of the Stern constant for Ca^+ ions, $K_{St,4}$ = 2.0 M^{-1}, determined in Ref. [4].

Appendix C. Final equilibrium film thickness, h_0

The model for calculation of the final equilibrium film thickness, h_0, is described in Ref. [3]. Below we summarize the main equations of the model, which are used in our calculations.

Adsorption equations for the film surfaces. The molecules at the film surfaces are in a chemical equilibrium with those in the bulk. Then, the adsorption equations for the molecules of the ionic and nonionic surfactant can be presented in the form [2]:

$$\frac{\alpha_{11}(\Gamma_1-\Gamma_2)}{1-\alpha_{\rm m}(\Gamma_1+\Gamma_{\rm n})}\exp[\frac{(2\alpha_{11}-\alpha_{\rm m})\Gamma_1+(2\alpha_{1n}-\alpha_{\rm m})\Gamma_{\rm n}}{1-\alpha_{\rm m}(\Gamma_1+\Gamma_{\rm n})}-\frac{2}{k_{\rm B}T}(\beta_{11}\Gamma_1+\beta_{1n}\Gamma_{\rm n})]$$

$$=K_1\gamma_{\pm}c_1\exp(-\Phi_{\rm s}) \qquad \text{(C1)}$$

$$\frac{\alpha_{\rm nn}\Gamma_{\rm n}}{1-\alpha_{\rm m}(\Gamma_1+\Gamma_{\rm n})}\exp[\frac{(2\alpha_{1n}-\alpha_{\rm m})\Gamma_1+(2\alpha_{\rm nn}-\alpha_{\rm m})\Gamma_{\rm n}}{1-\alpha_{\rm m}(\Gamma_1+\Gamma_{\rm n})}-\frac{2}{k_{\rm B}T}(\beta_{1n}\Gamma_1+\beta_{\rm nn}\Gamma_{\rm n})]=K_{\rm n}c_{\rm n} \qquad \text{(C2)}$$

Γ_1 is the adsorption and K_1 is the adsorption constant of the ionic surfactant; $\Gamma_{\rm n}$ and $K_{\rm n}$ are the analogous quantities for the nonionic surfactant; Γ_2 is the adsorption of counterions bound in the Stern layer. The concentrations c_1, c_2, and $c_{\rm n}$ are those calculated by using the model in Appendix B. The bulk activity coefficient $\gamma_{\pm}$ is defined by Eq. (B9). The dimensionless surface potential is $\Phi_{\rm s}\equiv|e\varphi_{\rm s}|/(k_{\rm B}T)>0$. In general, the value of $\Phi_{\rm s}$ at the film surface is different from the micelle surface potential. The excluded areas, α_{11} and $\alpha_{\rm nn}$, and the interaction parameters accounting for tail-tail interaction of van der Waals origin, β_{11} and $\beta_{\rm nn}$, are known parameters obtained in Ref. [2] by processing of surface tension isotherms; see Table C1.

According to the two-component van der Waals model for the surface pressure, the mean excluded area, $\alpha_{\rm m}$, is defined as follows:

$$\alpha_{\rm m}(\Gamma_1+\Gamma_{\rm n})^2\equiv\alpha_{11}\Gamma_1^2+2\alpha_{1n}\Gamma_1\Gamma_{\rm n}+\alpha_{\rm nn}\Gamma_{\rm n}^2 \qquad \text{(C3)}$$

The parameters α_{1n} and β_{1n} are calculated from the relationships:

$$\alpha_{1n}=(\frac{\alpha_{11}^{1/2}+\alpha_{\rm nn}^{1/2}}{2})^2\ ,\ \beta_{1n}=\beta_{11}(\frac{\alpha_{11}}{\alpha_{1n}})^{3/2} \qquad \text{(C4)}$$

The Stern isotherm, describing the adsorption of counterions at the headgroups of the ionic surfactant, reads:

$$\frac{\Gamma_2}{\Gamma_1 - \Gamma_2} = K_{\mathrm{St}} \gamma_{\pm} c_2 \exp \Phi_{\mathrm{s}} \tag{C5}$$

The occupancy of the Stern layer, θ, is defined as follows:

$$\theta \equiv \frac{\Gamma_2}{\Gamma_1} \tag{C6}$$

It is convenient to use the interaction parameters in their dimensionless form:

$$\hat{\beta}_{11} \equiv \frac{2\beta_{11}}{\alpha_{11} k_{\mathrm{B}} T} \ , \ \hat{\beta}_{\mathrm{nn}} \equiv \frac{2\beta_{\mathrm{nn}}}{\alpha_{\mathrm{nn}} k_{\mathrm{B}} T} \tag{C7}$$

Table C1 summarizes the values of the physicochemical parameters characterizing the adsorption layers at the film surfaces [2].

Table C1. Parameters of the adsorption isotherms for C*n*-SME and the nonionic admixture.

C*n*-SME	α_{11} (Å^2)	K_1 (M^{-1})	$\hat{\beta}_{11}$	α_{nn} (Å^2)	K_{n} (M^{-1})	$\hat{\beta}_{\mathrm{nn}}$
$n = 12$	37.0	5.916×10^4	1.47	22.6	7.450×10^4	6.75
$n = 14$	37.0	5.745×10^5	1.74	22.6	6.555×10^5	6.75
$n = 16$	37.0	5.543×10^6	1.98	22.6	5.665×10^6	6.75

Charge regulation at the film surfaces. To close the system of equations one needs the value of the electrostatic potential, Φ_{s}, at the film surface. It can be found using an equation, which relates the surface charge density and the surface electric potential [3]:

$$\Gamma_1 - \Gamma_2 = [\frac{1}{2\pi L_{\mathrm{B}}} F(\Phi_{\mathrm{s}}, \Phi_{\mathrm{m}})]^{1/2} \ , \ L_{\mathrm{B}} \equiv \frac{e^2}{4\pi\varepsilon\varepsilon_0 k_{\mathrm{B}} T} \tag{C8}$$

where L_{B} is the Bjerrum length, Φ_{m} is the dimensionless electrostatic potential at the film midplane; the function F originates from the first integral of the Poisson-Boltzmann equation:

$$F(\Phi_{\mathrm{s}}, \Phi_{\mathrm{m}}) = 2(c_1 + C_{\mathrm{A}})(\cosh \Phi_{\mathrm{s}} - \cosh \Phi_{\mathrm{m}}) + \alpha c_{\mathrm{mic}} (\exp \Phi_{\mathrm{s}} - \exp \Phi_{\mathrm{m}})$$

$$+ \frac{c_{\mathrm{mic}}}{N_{\mathrm{agg}}} [\exp(-\alpha N_{\mathrm{agg}} \Phi_{\mathrm{s}}) - \exp(-\alpha N_{\mathrm{agg}} \Phi_{\mathrm{m}})] \tag{C9}$$

The principles of the computational procedure are as follows. The input parameters are α_{11}, α_{nn}, $\hat{\beta}_{11}$, $\hat{\beta}_{nn}$, K_1 and K_n (Table C1); α_{1n} and β_{1n} – see Eqs. (C4) and (C7); C_A, c_1, c_n, c_{mic}, α, and N_{agg} are determined as explained in Appendix B.

In the case of *single interface* in contact with micellar solution, we have $\Phi_m \equiv 0$, and then the five unknown variables, Γ_1, Γ_2, Γ_n, Φ_s, and α_m, are to be determined from the following system of five equations, Eqs. (C1), (C2), (C3), (C5), and (C8). The problem is solved numerically; see, e.g., Ref. [3].

In the case of *thin liquid film* of given thickness h, the electric potential in the film midplane, Φ_m, appears as an additional unknown variable, and the system of equation has to be upgraded with an additional equation originating from the second integral of Poisson-Boltzmann equation [3]:

$$\int_{\Phi_m}^{\Phi_s} \frac{d\Phi}{F(\Phi_s,\Phi_m)^{1/2}} = (2\pi L_B)^{1/2}(h-h_a) \tag{C10}$$

Here, $h - h_a$ is the thickness of the film's aqueous core; h is the experimental film thickness, which includes the two surfactant adsorption layers, each of them of thickness $h_a/2$. The integral in the left-hand side of Eq. (C10) has no analytical solution. It is solved numerically using an appropriate change of the integration variable to avoid the weak singularity at $\Phi = \Phi_m$.

Calculation of the final equilibrium film thickness, h_0. In our experiments performed in a SE cell, the final film equilibrium thickness, h_0, corresponds to capillary pressure, P_c, which is counterbalanced by the disjoining pressure, Π. The main components of disjoining pressure are the van der Waals and electrostatic components, $\Pi = \Pi_{vw} + \Pi_{el}$. Then, the mechanical equilibrium at the film surfaces yields the following equation for h_0:

$$\Pi_{vw}(h_0) + \Pi_{el}(h_0) = P_c \tag{C11}$$

The theoretical expression for Π_{vw} is given in Ref. [3]. The expression for Π_{el} is [3]:

$$\frac{\Pi_{el}(h_0)}{k_B T} = 2(c_1 + C_A)(\cosh\Phi_m - 1) + \alpha c_{mic}(\exp\Phi_m - 1) - \frac{c_{mic}}{N_{agg}}[1 - \exp(-\alpha N_{agg}\Phi_m)] \tag{C12}$$

Eq. (C12) presents Π_{el} as the difference between the osmotic pressures in the film midplane and in the bulk of solution. In order to determine h_0, Eq. (C11), along with the expressions for

$\Pi_{wv}(h_0)$ and $\Pi_{el}(h_0)$, is to be added to the system of equations described above. One has to set $h = h_0$ in Eq. (C10). Description of the numerical procedures can be found in Refs. [1–3]. The capillary pressure P_c is an input parameter known from the experiment; one could use the approximation $P_c \approx 2\sigma/R_{in}$, where R_{in} = 1.5 mm is the inner radius of the SE cell, and σ is the solution's surface tension.

References cited in this Supplementary Material

[1] K.D. Danov, P.A. Kralchevsky, K.P. Ananthapadmanabhan, Micelle-monomer equilibria of ionic surfactants and in ionic-nonionic mixtures: A generalized phase separation model, Adv. Colloid Interface Sci. 206 (2014) 17–45.

[2] K.D. Danov, R.D. Stanimirova, P.A. Kralchevsky, E.S. Basheva, V.I. Ivanova, J.T. Petkov, Sulfonated methyl esters of fatty acids in aqueous solutions: Interfacial and micellar properties, J. Colloid Interface Sci. 457 (2015) 307–318.

[3] S.E. Anachkov, K.D. Danov, E.S. Basheva, P.A. Kralchevsky, K.P. Ananthapadmanabhan, Determination of the aggregation number and charge of ionic micelles from the stepwise thinning of foam films, Adv. Colloid Interface Sci. 183–184 (2012) 55–67.

[4] V.I. Ivanova, R.D. Stanimirova, K.D. Danov, P.A. Kralchevsky, J.T. Petkov, Sulfonated methyl esters, linear alkylbenzene sulfonates and their mixed solutions: Micellization and effect of Ca^{2+} ions, Colloids Surf. A 519 (2017) 87–97.